Journal of Building Engineering 98 (2024) 111069

Contents lists available at ScienceDirect

Journal of Building Engineering

journal homepage: www.elsevier.com/locate/jobe

Flexural properties of fiber-reinforced concrete using hybrid recycled steel fibers and manufactured steel fibers

Tohid Asheghi Mehmandari [a], Mehdi Shokouhian [b], Mohammad Zakeri Josheghan [c], Seyed Ali Mirjafari [a], Ahmad Fahimifar [a], Danial Jahed Armaghani [d,*], Kong Fah Tee [e,f,**]

[a] Department of Civil and Environmental Engineering, Amirkabir University of Technology (Tehran Polytechnic), Tehran, Iran
[b] Department of Civil Engineering, Morgan State University, Baltimore, United states, USA
[c] Department of Civil, Chemical, Environmental and Materials Engineering, University of Bologna, Bologna, Italy
[d] School of Civil and Environmental Engineering, University of Technology Sydney, Sydney, NSW, 2007, Australia
[e] Department of Civil and Environmental Engineering, King Fahd University of Petroleum and Minerals, Dhahran, 31261, Saudi Arabia
[f] Interdisciplinary Research Center for Construction and Building Materials, KFUPM, Dhahran, 31261, Saudi Arabia

ARTICLE INFO

Keywords:
Hybrid fiber reinforced concrete
Recycled steel fiber
Flexural performance
Digital image correlation
Computed tomography (CT scan)
Scanning electron microscopy

ABSTRACT

This study investigates the flexural properties of fiber-reinforced concrete (FRC) using a hybrid mix of recycled steel fibers (RSF) from waste tires and manufactured steel fibers (MSF). The aim of this study is to demonstrate hybrid steel fiber reinforcement as a more environmentally sustainable alternative to traditional single-fiber systems, by assessing whether hybrid reinforcement can achieve or surpass the performance of conventional single-manufactured steel fiber reinforcement. Using a novel four-stage methodology, this paper presents a comprehensive and detailed evaluation of mechanical and ductility performance through three-point bending tests, digital image correlation (DIC), CT-scans, and scanning electron microscopy (SEM). The results from flexural stress-deflection curves were used to evaluate the flexural strength and toughness. This was followed by an in-depth eight-stage DIC analysis and Surface Damage Index (SDI) curves throughout the test. CT-scan images were used to quantify the proportion of fibers classified as pulled-out, ruptured, or bridging the crack, while SEM analyzed the efficiency of fiber reinforcement through microstructural evaluations, further validating the findings of this study. Results show that hybrid reinforcement significantly enhances both toughness and ductility while reducing surface damage. MSFs in the hybrid system improve post-peak ductility and energy absorption by bridging large cracks, while RSFs prevent micro-cracks, increasing pre-peak rigidity. CT-scan analysis reveals that the inclusion of RSFs reduces pulled-out MSFs by 26 %, further boosting flexural performance. SEM confirms the superior bond of MSFs with the concrete matrix in hybrid samples. Additionally, higher fiber content in FRC enhances toughness and ductility while reducing surface damage. This research advances our understanding of hybrid fiber-reinforced concrete and promotes more sustainable construction practices through the use of recycled steel fibers. By leveraging the combination of new methodologies, the study effectively targets gaps in the current research landscape, offering a comprehensive approach to improving performance and sustainability in construction materials.

* Corresponding author.
** Corresponding author. Department of Civil and Environmental Engineering, King Fahd University of Petroleum and Minerals, Dhahran, 31261, Saudi Arabia.
E-mail addresses: danial.jahedarmaghani@uts.edu.au (D. Jahed Armaghani), tee.fah@kfupm.edu.sa (K.F. Tee).

https://doi.org/10.1016/j.jobe.2024.111069
Received 30 July 2024; Received in revised form 20 September 2024; Accepted 12 October 2024
Available online 15 October 2024

1. Introduction

Concrete, a widely used material in civil engineering, has inherent vulnerabilities due to its low tensile strength compared to its compressive strength, making it susceptible to cracking and failure under tensile stress, but resistant to compression. The use of fiber-reinforcing materials is widely acknowledged as an effective method for improving the mechanical and ductile characteristics of concrete, particularly when hybrid fibers are used to improve the properties of plain concrete. This method for improving the overall performance of concrete has achieved global appeal [1–7].Steel fibers in various geometric shapes, such as hooked, crimped, undulated, and others, are widely available on the market [8–10]. The mechanical properties of steel fibers and the performance of FRC can be affected by their shape. Hooked fibers, for example, can improve the anchoring effect and interlocking between the fibers and the matrix, whereas crimped fibers can strengthen the fiber-to-matrix interaction [11]. In addition to Manufactured Steel Fiber (MSF), Recycled Steel Fiber (RSF) has gained popularity in recent years due to its environmental benefits and low cost. The environmental benefits and cost-effectiveness of recycled steel fiber have piqued the interest of researchers, construction companies, and planners making it a popular choice in industry. According to these investigations, recycled tire waste fibers' tensile, flexural, and fiber-to-matrix adhesion characteristics are comparable to conventional steel fibers used in concrete. Moreover, RSF increases the material's ability to absorb energy by bridging and prevents lateral cracks [12–14]. It is noteworthy that the disposal of over 500 million used tires into landfills poses a significant threat to society, not only due to the limited availability of land disposal sites [15] but also because the accumulation of solid tire waste has been associated with potential health risks [16,17]. In fact, the recycling of used tires has the potential to prevent approximately 1.52 tons of CO2 emissions per year [18]. Experimental research has demonstrated that the incorporation of recycled steel fibers into concrete enhances various structural properties, including flexural strength [19]. FRC can be classified into single-fiber reinforced concrete and Hybrid Fiber Reinforced Concrete (HFRC), which incorporates two or more fiber types. In general, HFRC has superior mechanical performance compared to single-fiber reinforced concrete. As a result of their complementary and cumulative contributions to the performance of the concrete mixture [20–25], the hybridization of fibers could maximize the enhancements brought about by fiber reinforcement. These enhancing effects are dependent on the variety of fiber, hybrid ratio, and fiber volume content. The selection of the suitable types of fibers and proportions of fibers for HFRC is contingent on a number of criteria, including the intended application, the needed mechanical qualities, the availability of the fibers, and the cost of the fibers [26–28] Worth noting the hybridization of recycled and industrial steel fibers can provide a cost-effective and sustainable solution for fiber-reinforced concrete. In light of the outlined advantages, and alignment with the contemporary introduction of hybridization strategies incorporating both recycled and manufactured steel fibers, it becomes imperative to pursue a thorough and comprehensive investigation into the physical, mechanical, and deformation characteristics of HFRC across both microstructural and macrostructural approach through rigorous experimental inquiry employing esteemed methodologies such as Digital Image Correlation, Computer Tomography (CT) Scanning, and Scanning Electron Microscopy (SEM). Digital Image Correlation (DIC) is a computer vision technique used to measure the formation and propagation of cracks in concrete materials. It captures digital images before and during loading and analyzes them using correlation techniques to determine properties like surface displacements, strain components, and crack opening and sliding displacements, load-point displacement, crack length, and crack tip location [29–31]. When M. Maglad et al. investigated the effect of fiber volume content (Vf) on the fracture behavior of steel fiber-reinforced concrete (SFRC) under flexural loading, they found that increasing the fiber content, from 0.5 % to 1.5 %, led to a 43 % increase in the maximum failure load and a 165 % increase in mid-span deflection, compared to specimens with lower fiber content [32].Using DIC, Yates et al. [33] quantified the crack tip displacement fields. Strauss Rambo et al. [34] used DIC to study the cracking and full field distribution of tensile strain for textile-reinforced refractory concrete. The results indicated three distinct zones of cracking patterns. Utilizing computed tomography (CT) scan technology for investigating the internal microstructure of matter is an extremely beneficial endeavor. With respect to fiber-reinforced concrete, it serves as a basis for comprehending the interactions among the concrete's internal microstructure. CT stands out as a non-destructive methodology pivotal for visualizing the intricate internal microstructure of materials, leveraging X-ray technology. A CT-Scan apparatus encompasses an intensity-controlled X-ray source alongside a highly sensitive detector adept at discerning even minute losses in X-ray intensity. Throughout the scanning process, X-rays are emitted omnidirectionally, permeating every point of the sample from myriad angles. The detector meticulously gauges and records the aggregate X-ray intensity of all emissions. While conventionally utilized in medical diagnostics, CT-Scan technology has found a burgeoning application in concrete research, particularly in the field of fiber-reinforced concrete (FRC) [35–43]. A paramount advantage of employing CT-Scan technology in FRC analysis lies in its unparalleled capability to precisely ascertain the position and orientation of each individual fiber [44]. Moreover, given the susceptibility of recycled fibers to pull-out phenomena, a chief concern among researchers, CT facilitates not only the investigation of pull-out percentages and ruptured fibers but also enables the determination of fiber volume content effect on fracture mechanisms in FRC. Such insights are otherwise unattainable without the finesse of CT imaging. Understanding the quantity and location of pull-out and ruptured fibers is of paramount importance, since the interaction between fibers and concrete is a significant factor contributing to these failures. To delve into this critical issue and comprehend the microcracks induced by fiber addition, it is imperative to analyze the Fiber Interface Transition Zone (FITZ). Micro-cracks within this zone are pivotal in initiating crack formation, capable of rapid expansion during seismic events or gradual propagation over time, thereby posing significant risks to structures [45–49].Conventionally, the initiation of cracks in concrete is believed to occur at the interface where aggregates and the cement paste meet, often preceding actual aggregate fragmentation [50–52]. This interface, known as the Interfacial Transition Zone (ITZ), extends approximately 30–50 μm from aggregates and is characterized by a plethora of microcracks, necessitating measures to effectively delay detachment between the cement paste and aggregates [53]. In Fiber Reinforced Concrete, the FITZ emerges as a crucial region surrounding the fibers, approximately 30 μm in extent. This zone is susceptible to

separation between the concrete matrix and steel fibers, potentially occurring prior to material failure [54–56]. To elucidate the microstructure and morphology of both the ITZ and FITZ, Scanning Electron Microscopy serves as a valuable tool. It provides insights into bond quality, porosity, and interface properties among aggregate particles, fibers, and cement paste, thereby enriching our comprehension of FRC performance. A comprehensive understanding of hybrid fiber-reinforced concrete (HFRC) systems requires integrating various perspectives from the existing body of research, particularly on the use of both manufactured and recycled steel fibers. Although individual studies have explored the benefits of single-fiber systems, they often focus on specific aspects such as flexural strength or microstructural behavior without offering a holistic approach. This paper unifies these perspectives by considering the complementary roles of recycled and manufactured fibers in enhancing both the mechanical properties and sustainability of concrete. Also, the existing literature has shown a lack of comprehensive investigation into the synergistic effects of combining recycled fibers, specifically those derived from automobile waste tires, with manufactured steel fibers in Hybrid Fiber Reinforced Concrete (HFRC). Moreover, The interaction between fibers and the concrete matrix is crucial for FRC performance. New methodologies, such as CT-scanning, offers an effective, non-destructive way of studying fiber distribution, pull-out, and microcracks in the concrete matrix, providing essential insights for optimizing fiber types and ratios to enhance FRC durability. This novel approach presents significant advantages in terms of environmental friendliness and cost-effectiveness. The methodology in question in this study comprises four interrelated and complementary stages. Initially, the experimental framework aims to conduct a comprehensive experimental program designed to analyze the mechanical and ductility performance of reinforced concrete. This analysis utilizes a hybrid combination of recycled and manufactured fibers, alongside single-fiber mixtures, incorporating varying fiber volume percentages from high to low values, under flexural loading conditions. Building on the insights from the initial analysis, the second stage seeks to gain detailed insights into the behavior of single-fiber and hybrid fiber reinforced concrete during the loading process and to identify a unique indicator termed the Surface Damage Index (SDI). This stage involves the use of a high-speed camera system in conjunction with digital image correlation analysis via MATLAB. Evaluating the SDI provides additional data on the surface conditions of the FRC samples, offering critical information on the crack propagation and surface damage characteristics of the material. Continuing from the surface-level analysis, the third stage employs CT-Scan technology to delve deeper into the material's internal structure. This stage examines the percentages of pull-out or ruptured fibers and assesses the impact of hybridization on the fracture mechanism of Fiber Reinforced Concrete (FRC), with analysis conducted using the Avizo application. This evaluation provides deeper insights into the interaction between fibers and the concrete matrix within the FRC samples, elucidating the complex dynamics and overall performance of these components during mechanical stress. Finally, to complement the macro and micro-level analyses, the fourth stage utilizes Scanning Electron Microscopy (SEM) to understand how microcracks in the Fiber Interface Transition Zone (FITZ) can initiate cracks in fiber reinforced concrete. The SEM analysis offers a detailed view of the microstructural interactions between the fibers and the concrete matrix, revealing the behavior of individual fibers within various mix designs. This comprehensive image helps to pinpoint the exact mechanisms of fiber performance and failure in the composite material.

1.1. Research significance

This study aims to provide a well-rounded analysis, by evaluating the flexural performance of hybrid fiber reinforced concrete from four various perspectives, with each method reinforcing the findings of the others. By utilizing a comprehensive approach, the research offers a deeper understanding of hybrid fiber-reinforced concrete, highlighting both its macro-level performance and micro-level interactions. This integrated evaluation ensures that different aspects of the material's behavior are thoroughly explored, leading to a more reliable and complete assessment of its structural benefits. Ultimately, this holistic approach contributes to advancing the development of more resilient and sustainable construction materials.

2. Materials and test method

2.1. Materials

For the study, CEM I 52.5N [57] Portland cement from Shahrekord Cement Industries Company was used, with its characteristics detailed by the manufacturer in Table 1. A polycarboxylic ether-based superplasticizer (SP) from S. Shimi Sakhteman was added in proportions of 0.2 %–2 %. All mixes used crushed limestone aggregate from the Raziabad mine in Tehran, with a maximum grain size of 19 mm, confirmed by an ASTM C136/C136M − 19 sieve analysis [49]. Fig. 1 displays the aggregate size limits, with a maximum allowable size of 19 mm. The study also incorporated two fiber types from Faratav Company: Manufactured 5D Hooked end steel fibers and Recycled tyre steel fibers, with their shapes and mechanical properties tested in a verified strength of materials lab as per manufacturer guidelines, shown in Fig. 2 and Table 2.

2.2. Mix design

Table 3 outlines the mix ratios for seven different mixes, all with a 0.340 water-to-binder ratio, including plain concrete (PC) and combinations of 4 single and 2 hybrid fiber-reinforced mixtures with total fiber contents of 0.25 % and 0.5 % by volume fraction (vf), categorized as low-fiber and high-fiber, respectively. "PC" denotes the fiber-free plain concrete mix design, while other mixes incorporate MSF, RSF, or both. Among the fiber-reinforced designs, three are low-fiber (0.25 % vf) and three are high-fiber (0.5 % vf), with mixed descriptions using 'M' for Manufactured and 'R' for Recycled fibers. The number following these letters (e.g., 0, 1.25, and 2.5) represents 10 times the fiber content as a percentage. For example, "M1.25R1.25″ includes 0.125 % RSF and 0.125 % MSF, totaling a

Table 1
Chemical, physical and mechanical properties of the cement used in this study.

Chemical properties	CaO	63.7 %
	Free CaO	1.19 %
	SiO_2	20.46 %
	Al_2O_3	5.57 %
	Fe_2O_3	3.65 %
	MgO	1.32 %
	SO_3	1.84 %
	K_2O	0.32 %
	Na_2O	0.49 %
	IR	0.46 %
	LOI	0.95 %
Physical properties	Initial setting time	195 min
	Final setting time	230 min
	Specific gravity	3.05 gr/cm^3
	Belin Number	2580 cm^2/gr
	Passing of 45-μm sieve	88.32 %
Compressive strength (MPa)	After 7 days	50.6
	After 28 days	61.6

0.25 % fiber content, classifying it as low-fiber. The experimental variables, particularly the steel fiber hybridization and variations in fiber content, were selected based on recommendations from the literature review, with careful consideration of the potential effects on workability and casting, ensuring they were appropriate for the scope of this study.This study also evaluated the slump, and flexural strength of the mixes using standard-sized aggregates and laboratory conditions, adding SP to the mixes at a rate of 0.5 %–1 % by weight of cement and mixing in a pan mixer. In order to evaluate the workability of the plain concrete and FRC mixtures, unit weight and slump experiments on fresh concrete were performed.

Initially, cement, aggregates were dry mixed for 2 min, followed by adding SP and water for 3 min, then fibers were mixed in for another 3 min to ensure thorough distribution within the mix. The mix was then cast into beam molds, vibrated on a shaking table to eliminate air pockets, and left in the molds for 24 h. The specimen fabrication was carried out by pouring the fiber reinforced concrete into a beam mold positioned at a 35-degree angle relative to the horizontal. Subsequently, specimens were water-cured at 20 ± 2 °C for 28 days. For strength evaluations, each mix was represented by three beams (500 mm*100 mm*100 mm), with results averaged across three samples per mix type. Also, the compressive, and splitting tensile strength of plain concrete was determined by averaging the results from three cylindrical samples (200 mm × 100 mm) for each test. Fig. 3 presents the (a) stress-strain diagram of the plain concrete in compression, and (b) stress-displacement diagram of the plain concrete in tension, illustrating its properties. The uniaxial compressive test, and splitting tensile results of plain concrete samples are aso provided in Table 4. Deflections of beams under three-point loading were measured using one LVDT at the midspan. The tests utilized Dartec-9600 servo control devices with a maximum capacity of 1000 kN in Amirkabir University of Technology's Rock Mechanics Laboratory. The three-point bending test, conducted in accordance with ASTM C1609/C1609M [58], mimics real-world bending forces concentrated at a single point or over a short area, providing a realistic condition assessment. It's important to mention that in this study, scaled specimens were utilized to replicate the mechanical behavior of fiber-reinforced concrete (FRC) while adhering to the practical constraints of laboratory testing. Scaling techniques, widely used in structural and material testing, provide valuable insights under controlled and repeatable conditions. Larger FRC members often present flaws or variations in fiber distribution, and scaling becomes crucial when the material exhibits nonlinear behavior, such as cracking, fiber bridging, and post-cracking behavior, as these factors can differ between large and small specimens, especially in post-peak responses [59].

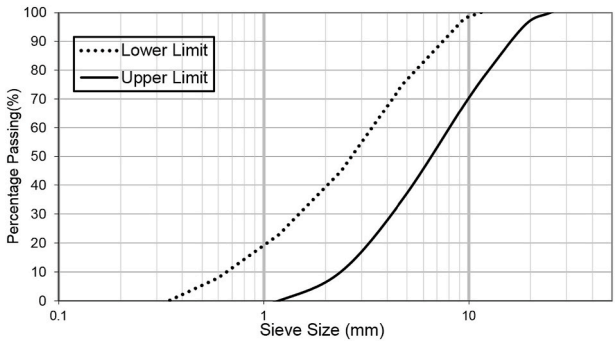

Fig. 1. Sieve analysis.

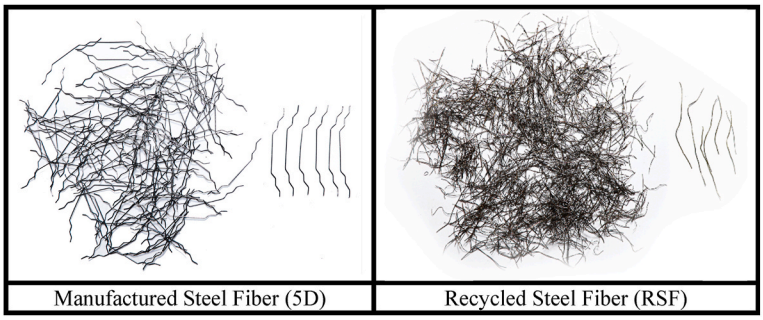

Fig. 2. Appearance of the fibers used in the test.

Table 2
The geometrical and mechanical properties of fibers.

Type	Length (mm)	Diameter (mm)	Aspect Radio (length/Diameter)	Tensile strength (MPa)	Specific gravity	Elastic modulus (GPa)
MSF	35	0.4	87.5	2830	7.8	210
RSF	20–40	0.35	57–114	3120	6.9	210

Table 3
The mixtures proportions of the control and FRC mixes.

Reinforcing Type	Mix Description	C (kg/m^3)	W (kg/m^3)	CS (kg/m^3)	FS (kg/m^3)	MSF (kg/m^3)	RSF (kg/m^3)	SP (kg/m^3)
–	PC	500	174.36	671.2	1013.4	0	0	2.8
Single	$M_{2.5}R_0$	500	174.36	671.2	1009.5	19.5	0	2.8
Hybrid	$M_{1.25}R_{1.25}$	500	174.36	671.2	1009.5	9.75	8.625	2.8
Single	$M_0R_{2.5}$	500	174.36	671.2	1009.5	0	17.25	2.8
Single	M_5R_0	500	174.36	666.2	1005.8	39	0	3.3
Hybrid	$M_{2.5}R_{2.5}$	500	174.36	666.2	1005.8	19.5	17.25	3.3
Single	M_0R_5	500	174.36	666.2	1005.8	0	34.5	3.3

C = Cement; W = Water; CS = Coarse Sand; FS = Fine Sand; MSF = Manufactured Steel Fiber; RSF = Recycled Steel Fiber; SP = Super Plasticizer.

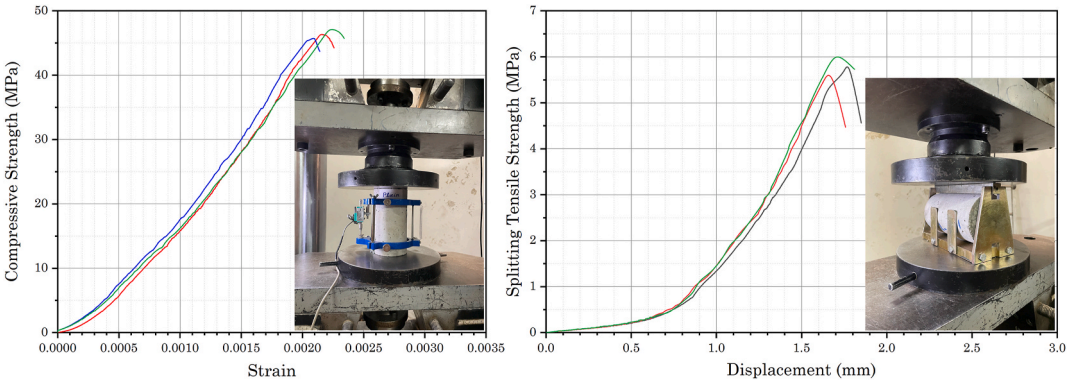

Fig. 3. (a) uniaxial compressive stress-strain, (b) splitting tensile stress-displacement diagram of plain concrete.

Table 4
Uniaxial Compressive test, and splitting tensile test results of plain concrete.

Mix		Plain		Mix		Plain	
Sample No.	1	2	3	Sample No.	1	2	3
Peak Load in Uniaxial Compressive test (kN)	370.56	359.06	363.86	Peak Load in Splitting Tensile test (kN)	189.8	181.38	185.08
Compressive Strength (MPa)	47.18	45.72	46.33	Splitting Tensile Strength (MPa)	6.04	5.77	5.89
Average Compressive Strength (MPa)		46.41		Average Splitting Tensile Strength (MPa)		5.9	
Standard Deviation		0.6		Standard Deviation		0.109	

2.3. DIC measurement

Digital Image Correlation, a non-contact, high-precision optical measurement technique, was used to monitor crack formation and distribution of cracks across specimens, and to back-calculate the strain distribution throughout the specimen. High-quality images required special preparation as follows [59,60]. All beam side sections were dotted at 1-cm intervals in three colors. A professional digital camera with a 1/2.8" 3M Sony IMX036 CMOS sensor was mounted on a tripod to reduce movement, recording the loading process from start to finish. Despite daylight testing, adjustable lighting from a projector, shown in Fig. 4, ensured consistent contrast. Videos, captured from the onset of loading, were edited using Aoao software, extracting 200 images per video for analysis. Ncorr [50], a free, high-quality DIC software, analyzed these images to assess strain distribution and crack behavior.

2.4. CT-scanning process

Computed tomography (CT) scans were conducted to observe the internal microstructure of Fiber Reinforced Concrete specimens after undergoing loading procedures for the current investigation. Due to constraints inherent in the hospital scanning setup, rather than conducting a comprehensive scan of the entire specimen, only a segment was examined, precisely selected from the central area surrounding the crack. The CT-scan system employed integrates an intensity-controlled X-ray source and a detector that measures the attenuation of X-ray intensity. During scanning, X-rays are emitted while a detector records the final X-ray intensity for all rays [62, 63]. In this study, a SIEMENS CT system equipped with a 130 kV, 130 mAs X-ray tube, located at Tehran's Tandis Multi Super Specialty Hospital, was utilized. Post-processing was conducted using "Avizo" software to extract 512 2D slices from each sample. The software generated a 3D image of the specimens by incorporating all acquired images. Each voxel of this three-dimensional object was assigned a grey level based on the material density at that point, ranging from 0 to 255, where 0 represents pure black and 255 represents pure white. Dark grey voxels and light grey voxels corresponded to less dense and denser points, respectively, such as steel fibers. The outcome of this initial post-processing step was a file containing the X, Y, and Z coordinates of each voxel's center along with its assigned grey level. The total number of voxels in each sample was approximately $9.5 \times 10\hat{}7$. Fig. 5 illustrates the aforementioned CT-scanning process.

2.5. Scanning electron microscopy

In this study, Scanning Electron Microscopy was utilized for the analysis of micro-cracks in FTIZ. The SEM was employed after loading, and the analysis involved image processing and CT-scan processing. The FRC sample is prepared for Electron Microscopy by utilizing cutting, polishing, or fracturing procedures to expose the desired surface of interest [64]. Afterwards, a thin layer of conductive material is put to cover the sample. Then, the prepared sample is attached to a sample holder or stub and inserted into the SEM chamber. In order to ensure the stability of the electron beam, the chamber is subjected to a process of high vacuum evacuation. The process of generating an electron beam requires the utilization of an electron source, such as a tungsten filament or a field emission gun (FEG), which is directed towards the surface of the sample. The interaction between the electron beam and the sample leads to the release of secondary electrons, backscattered electrons, and distinctive X-rays [65]. The emissions offer essential information about the sample's surface shape, chemistry, and crystal structure. This approach enables the analysis of crack patterns and the interplay between concrete and fibers. The SEM utilizes detectors to gather released electrons or X-rays, which are subsequently transformed into electrical signals and presented on a screen for visual examination. The use of high-resolution imaging techniques allows for the capture of detailed visual information about the sample surface. Additionally, specialized software facilitates the quantitative analysis of the recorded photos. Fig. 6 depicts the SEM analysis methodology utilized in this investigation, using SEM in the main laboratory of Amirkabir University of Technology. It's worth mentioning that to minimize sample-specific bias, SEM images were obtained from various fiber-matrix regions across different samples. The analyzed regions consistently showed comparable characteristics, such as crack formation and fiber pullout, confirming that the presented SEM images accurately reflect the FITZ in FRC samples.

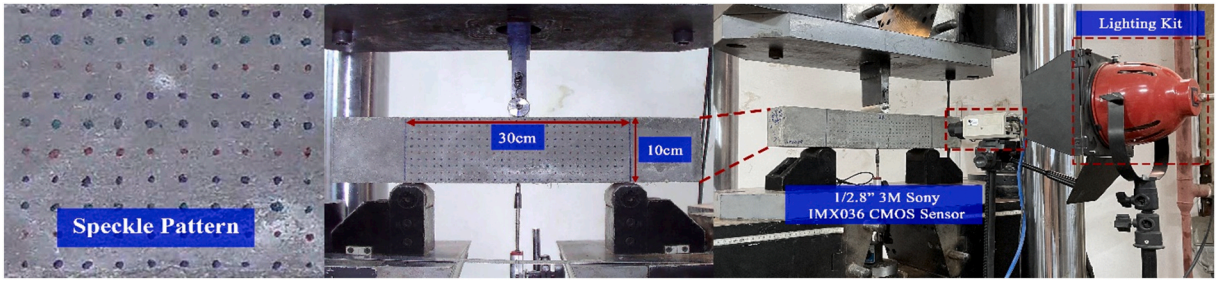

Fig. 4. DIC measurement setup.

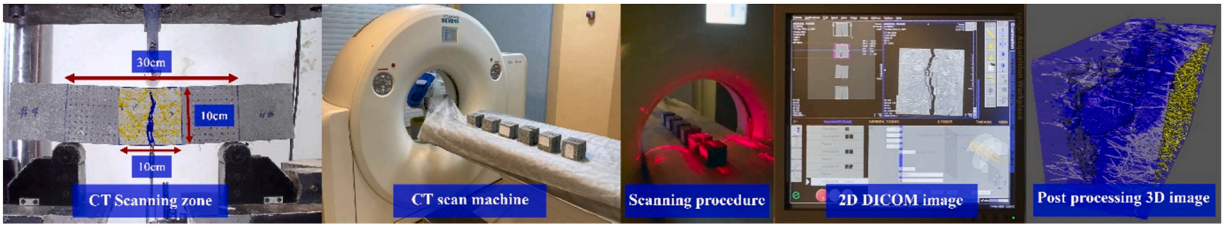

Fig. 5. CT-scan procedures.

Fig. 6. Scanning electron microscopy procedure.

3. Results and discussion

In this study, our focus is on the investigation of the physical, mechanical and ductility performance of recycled and hybrid fiber-reinforced concrete, focusing on flexural aspects of fiber-reinforced concrete. Results of the physical and mechanical properties of FRC samples are provided in Table 5 alongside the same characteristics related to plain concrete.

The "Results and Discussion" section is organized into three main parts. Initially, it examines the behavior of all samples subjected to the flexural tests, focusing on experimental data for analysis. Following this, the discussion shifts to examining the surface of samples through DIC analysis, where processed images and various behavioral curves, obtained from DIC results, are analyzed in detail. The third section concentrates on the microstructural evaluation of FRC samples, employing CT scanning and SEM to assess the efficiency of fiber reinforcement within the concrete matrix.

3.1. Experimental analysis of flexural performance

This section evaluates strength, ductility and toughness from three-point bending tests, alongside each sample's flexural behavior curve. These evaluations focus on two primary aspects: the influence of fiber content and the impact of the hybridization approach in fiber reinforcement.

The ASTM C 1609 [58] standard suggests analyzing flexural parameters at deflections of $\delta_{L/600}$ and $\delta_{L/150}$, where "L" is the span length of the beam, in this case corresponding to deflections of 0.5 mm and 2 mm, respectively. However, to fully understand flexural behavior, this approach has been deemed insufficient, leading to the introduction of two additional points, which are the flexural peak and the flexural ultimate point, for a more thorough evaluation. Toughness, defined by ASTM C 1609 as the area under the flexural stress-deflection curve, indicates a sample's energy absorption capability during testing. By employing the four critical points mentioned, four distinct toughness values are calculated: T_{pre} and T_{post} represent the areas under the curve from the start to the peak flexural strength point and from this peak to the ultimate deflection point, respectively. T_{600} and T_{150} are derived from the curve area from the start to the $\delta_{L/600}$ (0.5 mm) and $\delta_{L/150}$ (2 mm) deflection points. Fig. 7 provides a schematic overview of the indices used in this analysis.

Table 5
Physical and mechanical properties of plain and FRC specimens.

Mix Description	Unit Weight	Slump	Peak Load in Bending test	Deflection corresponding to peak load (δpeak)	Ultimate deflection (δu)	Flexural Strength	Increase
	(kg/m3)	(mm)	(kN)	(mm)	(mm)	(MPa)	(%)
PC	2378	105	13.71	0.205	0.205	6.17	0.0
$M_{2.5}R_0$	2378	92	27.00	0.635	6.155	12.15	96.92
$M_{1.25}R_{1.25}$	2375	86	24.56	0.575	6.52	11.05	79.09
$M_0R_{2.5}$	2382	75	23.29	0.43	4.80	10.48	69.85
M_5R_0	2375	73	27.16	0.84	8.00	12.22	98.05
$M_{2.5}R_{2.5}$	2371	90	25.53	0.58	6.805	11.49	86.22
M_0R_5	2369	75	23.80	0.36	7.03	10.71	73.58

Flexural strength (f) is determined using Eq. (1), with values at specific deflections serving as indices in this study: $f_{L/600}$, f_p, $f_{L/150}$, and f_u, corresponding to bending strengths at $\delta_{L/600}$ (0.5 mm), peak deflection (δ_{peak}), $\delta_{L/150}$ (2 mm), and ultimate deflection (δ_u), respectively. Equivalent Flexural Stress is a key metric used to assess the flexural performance of concrete. Equivalent Flexural Stress reflects the average stress a concrete specimen can endure during bending before failure, highlighting the influence of fiber reinforcement on the flexural properties of FRC

$$f = \frac{3pL}{2bh^2} \tag{1}$$

Fig. 8 shows flexural stress-deflection curves for plain and fiber-reinforced concrete (FRC) specimens, highlighting fibers' role in enhancing flexural capacity and ductility. Further details on flexural behavior improvement are discussed later.

Flexural test results of plain concrete and FRC samples are provided in Table 6, in details for each mix and sample Number. Table 7, alongside Fig. 9, details the flexural strength and toughness of plain and FRC specimens at four critical points, including T_{total}, which indicates the total energy absorption from the entire flexural stress-deflection curve. Plain concrete exhibits limited ductility, failing at a peak deflection of 0.203 mm, below the $\delta_{L/600}$ (0.5 mm) and $\delta_{L/150}$ (2 mm) thresholds, preventing further toughness evaluation at these stages. Fiber reinforcement boosts concrete ductility, as shown in Fig. 8 and Table 7. All 6 FRC specimens surpasses plain concrete in strength, ductility, and toughness. Plain concrete tends to fail abruptly, while FRC maintains strength and ductility at higher deflections, slows the decline in flexural stress, while enhancing flexural strength. This is reflected in toughness values, with plain concrete exhibiting low toughness due to brittleness, contrasting with FRC's notably higher toughness.

3.1.1. *Fiber content effect on flexural strength*

Fig. 9 shows that higher fiber content in single-fiber FRC samples significantly increases pre-peak strength (f600), reflecting crack initiation strength. FRCs with only RSF nearly doubled this strength with double the fiber content, while single-MSF samples saw a 28 % increase. In contrast, hybrid samples had only a marginal 3 % improvement. Regarding peak strength (f_p), none of the three approaches—single-MSF, single-RSF, and hybrid—show significant improvement in f_p, with hybrid samples displaying a modest 4 % increase at most. Yet, the presence of fibers distinctly enhances f_p compared to plain concrete, which obtains an f_p nearly 40 % lower than the lowest FRC specimen. The impact of fiber content on f_p is nuanced; too much fiber contents may negatively affect f_p by disrupting the aggregate-cement bond and causing a heterogeneous FRC behavior, leading to a weaker concrete matrix and reduced f_p at lower stress levels. Consequently, excessive fiber content is as detrimental as none in terms of f_p. Both 0.25 % vf and 0.5 % vf fiber

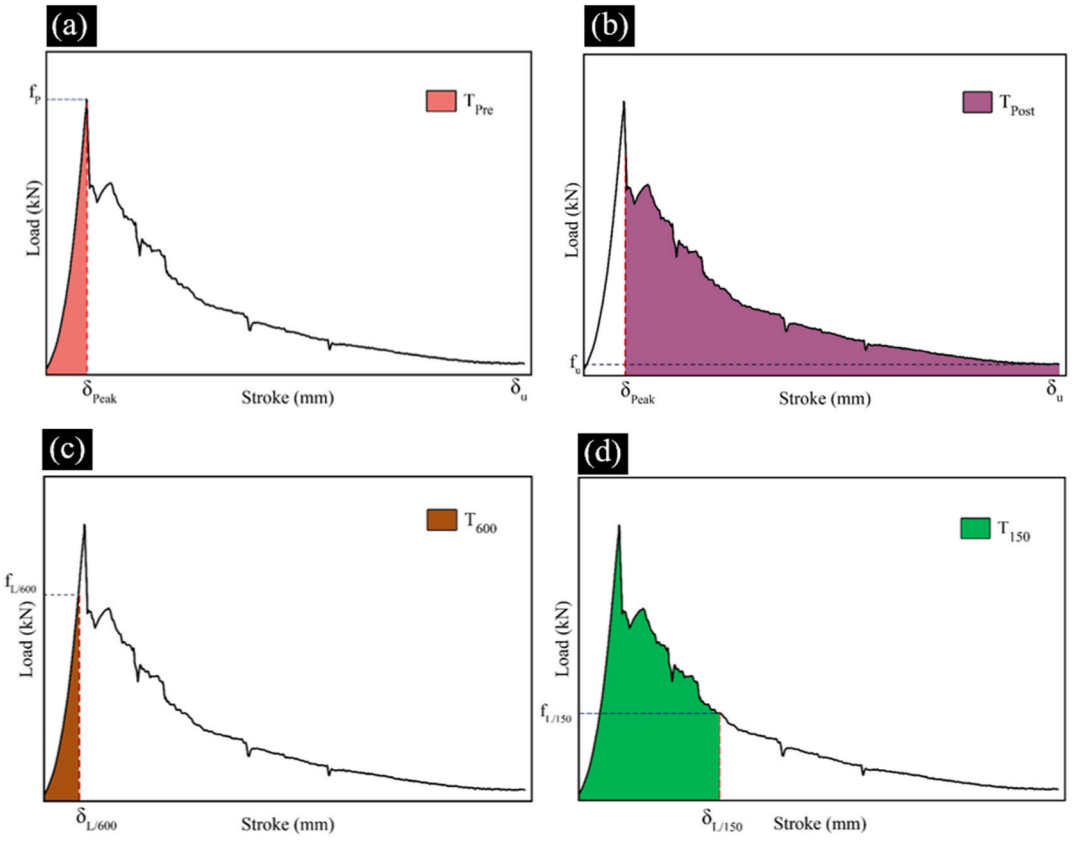

Fig. 7. Schematic view of various indices utilized in this study: (a) f_p and T_{pre}; (b) f_u and T_{post}; (c) $f_{L/600}$ and T_{600}; (d) $f_{L/150}$ and T_{150}.

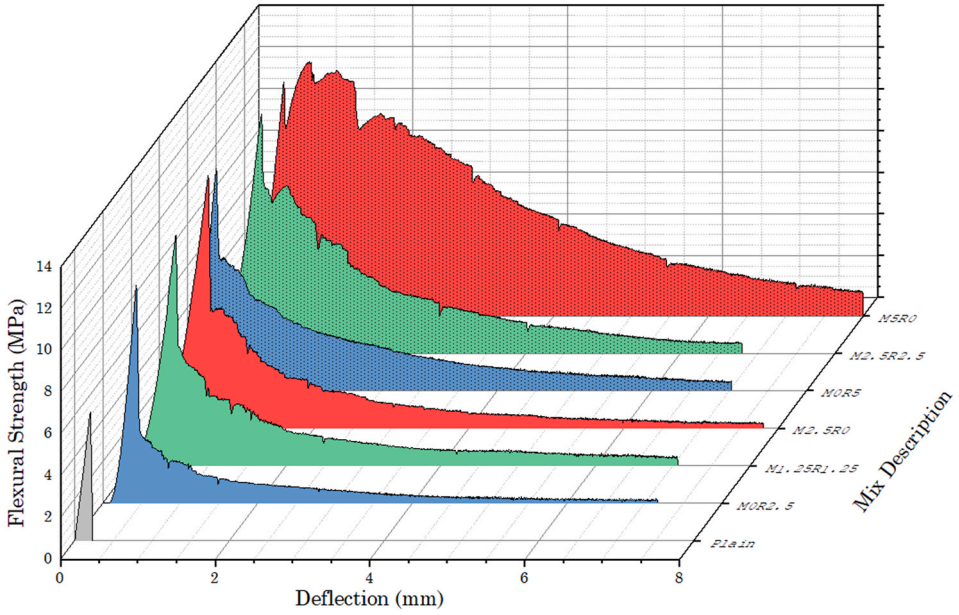

Fig. 8. Flexural stress-deflection curves of plain and FRC specimens.

Table 6
Flexural test results of plain concrete and FRC samples.

Mix	Plain			M2.5R0			M1.25R1.25			M0R2.5		
Sample No.	1	2	3	1	2	3	1	2	3	1	2	3
Peak Load in Bending test (kN)	13.60	13.85	13.68	26.89	27.01	27.10	25.51	23.56	24.60	23.19	23.38	23.30
Flexural Strength (Mpa)	6.12	6.23	6.16	12.10	12.15	12.20	11.48	10.60	11.07	10.43	10.52	10.49
Average Flexural Strength (Mpa)		6.17			12.15			11.05			10.48	
Standard Deviation		0.0464			0.0387			0.3579			0.0357	
Mix		M5R0			M2.5R2.5			M0R5				
Sample No.	1	2	3	1	2	3	1	2	3			
Peak Load in Bending test (kN)	27.03	27.34	27.10	25.30	25.75	25.55	23.48	23.90	24.02			
Flexural Strength (Mpa)	12.16	12.30	12.20	11.39	11.59	11.50	10.57	10.76	10.81			
Average Flexural Strength (Mpa)		12.22			11.49			10.71				
Standard Deviation		0.0602			0.0828			0.1042				

Table 7
Flexural strength and toughness indexes of plain and FRC specimens based on experimental results and ASTM C 1609 standard.

Mixture ID	$\delta_{L/600}$ (0.5 mm)		δ_{peak} (mm)		$\delta_{L/150}$ (2 mm)		δ_u(mm)		Total
	$f_{L/600}$ (MPa)	T_{600} (N m)	f_p (MPa)	T_{pre} (N.m)	$f_{L/150}$ (MPa)	T_{150} (N m)	f_u (MPa)	T_{post} (N.m)	T_{tota} (N.m)
PC	0	0	6.17	0.7258	0	0	0	0	0.7258
$M_{2.5}R_0$	8.46	1.5632	12.15	2.9586	2.07	8.0891	0.25	9.2704	12.229
$M_{1.25}R_{1.25}$	8.83	1.5198	11.05	2.2662	1.69	6.9678	0.42	8.7137	10.98
$M_0R_{2.5}$	3.25	1.7841	10.48	1.3882	0.91	4.2550	0.15	4.7999	6.188
M_5R_0	10.88	1.9342	12.22	5.6497	9.27	17.8014	1.09	35.4892	41.139
$M_{2.5}R_{2.5}$	9.08	1.7095	11.49	2.5411	3.65	11.1146	0.46	15.5125	18.0536
M_0R_5	6.21	2.4919	10.71	1.5691	2.51	8.1995	0.43	12.1011	13.6702

content achieve comparable f_p stresses, suggesting these can be near-optimal values for fiber contents for achieving optimal f_p. All samples showed significant improvement in post-peak strength (f_{150}) with increased fiber content. Specifically, single-MSF samples saw a 350 % increase in f_{150}, while single-RSF and hybrid samples also doubled their strength with higher fiber content. It's important to note that the improvement in f_{150} was anticipated, as the primary objective of fiber reinforcement is to enhance ductility and improve post-peak performance in concrete. These results underscore MSF's impact on the post-peak flexural strength of FRC specimens, attributed to the double-hooked ends of the fibers preventing complete pull-out and enhancing load resistance without losing bond to the concrete matrix. Additionally, their longer and bulkier structure, compared to RSFs, allows them to transfer stress across larger crack widths. This characteristic likely explains the significant improvement in f_{150} observed with increased fiber content. This is

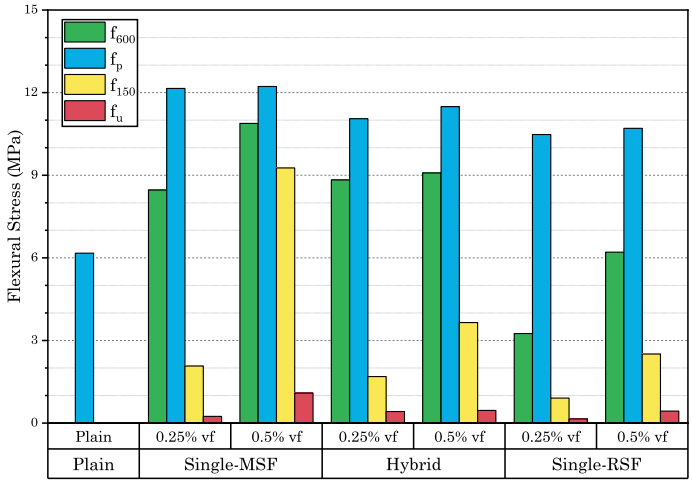

Fig. 9. Flexural pre-peak, peak, and post-peak strength of FRC samples.

particularly evident when comparing M2.5R0 and M5R0 samples, highlighting a marked enhancement in f_{150} with fiber content increase. All FRC samples, behave in a way that an ultimate strength (f_u) can be associated with them. However, the plain concrete sample shows brittle behaviour and no ultimate strength (f_u) can be recorded. In summary, while low-fiber FRC mixtures show similar performance to others in the elastic zone, high-fiber mixes have a much greater impact on post-peak (plastic) behavior. Both high- and low-fiber samples improve elastic and plastic behavior compared to plain concrete, but the higher fiber content is particularly effective in enhancing post-peak performance.

3.1.2. Hybridization effect on flexural strength

In the low-fiber group of FRC samples, the hybrid mixture's pre-peak flexural strength is notably higher than single-fiber samples. This superior performance suggests that the hybrid approach, leveraging both MSF and RSF, results in enhanced structural behavior under pre-peak loads. Although the peak strength of the hybrid M1.25R1.25 mix is on par with single-fiber mixtures, it is achieved with half the amount of MSFs used in M2.5R0, making it advantageous. Furthermore, the hybrid sample registers the highest ultimate flexural strength, indicating that the FRC sustains less damage when utilizing a combination of fiber types. However, in high-fiber samples, the hybrid approach of M2.5R2.5 led to an average outcome between single-MSF and single-RSF results. Yet, the f_{600} and f_p values show more similarity to the single-MSF approach. However, the f_{150} value in M2.5R2.5 is closer to M0R5 behavior. The results generally show that in higher fiber contents, which directly means higher MSF contents, the effect of manufactured fibers on the flexural post-peak behavior of FRC samples is much more significant. This statement first shows MSFs potential in improving post-peak ductility and then justifies the f_{150} values obtained in samples. Also, it's worth noting that all hybrid samples expressed higher pre-peak strength than plain concrete's peak strength. This states the higher resistance to crack initiation in hybrid mixes compared to plain concrete.

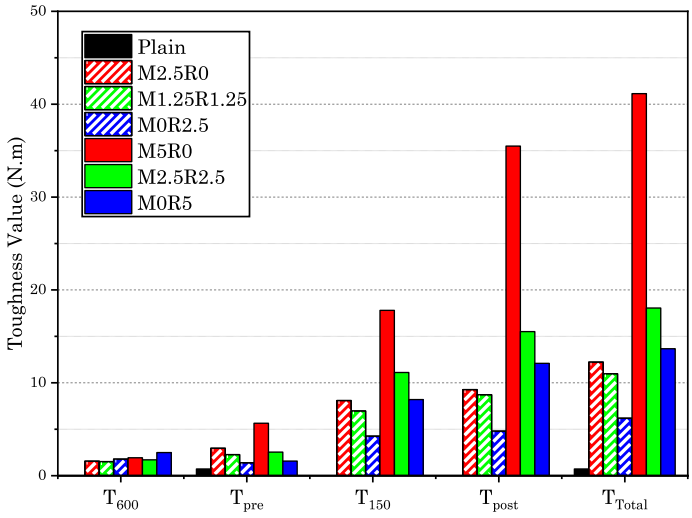

Fig. 10. Toughness indexes of plain and FRC samples.

3.1.3. Fiber content effect on flexural ductility

Fig. 10 showcases toughness indexes for seven different mix designs, focusing on the impact of steel recycled fibers and the hybrid reinforcement approach on the ductility and toughness of concrete specimens. Plain concrete, unable to withstand 0.5 mm displacement before breaking, registers a T_{600} of zero, indicating no ductility in the pre-crack zone.

In contrast, FRC samples exhibit greater ductility and displacement within the elastic and also non-elastic zones. Fig. 10 shows that doubling fiber content from 0.25 % to 0.5 % vf enhances T_{600} values across all samples. Notably, single-RSF samples see a 40 % T_{600} increase, while the M2.5R2.5 sample gains a 12.5 % increase over the M1.25R1.25. The M0R5 sample stands out with the highest T_{600} value, indicating a robust bond between recycled fibers and the concrete matrix, implying more energy is needed for crack initiation. This is supported by the high T_{600} value in the M0R2.5 sample compared to its low-fiber counterparts. T_{600} values suggests the potential of RSFs in postponing the creation of microcracks inside the concrete matrix. T_{pre} values, indicating toughness at peak strength, are minimal in plain concrete compared to FRC samples, underscoring the benefit of steel fibers in energy absorption and flexural ductility. Higher fiber contents correlate with increased T_{pre} values in both single-fiber and hybrid specimens. The M5R0 sample registers the highest T_{pre} value. Doubling fiber content typically doubles the T_{150} toughness value, as its clear from Fig. 10 and Table 7, with the least rise seen in hybrid samples. A key objective in fiber reinforcement is to enhance the ductility of concrete, particularly in the post-peak zone where it's most prevalent. Thus, it's expected that increased fiber content would notably improve post-peak toughness indexes. Single-MSF mixes demonstrate the largest gains in this regard, reaffirming their superiority in managing more significant cracks at greater deflections. The same statements are also true about T_{post} values achieved by FRC samples. M5R0 sample by attaining a 283 % increase in T_{psot}, predictably shows the highest increase in post-peak toughness index as a result of doubled fiber content. T_{total} values also rise significantly with increased fiber content, especially in single-MSF samples, indicating enhanced overall toughness. Overall, manufactured steel fibers show strong potential to enhance post-peak performance in FRC, with higher fiber content further increasing concrete's ductility. Fig. 11 shows the flexural behavior of FRC samples in a three-point flexural test, grouped by fiber content, where all FRC samples endure a minimum 6 mm displacement, significantly surpassing plain concrete's 0.2 mm. FRCs reach peak strength at around 1 mm displacement, highlighting fiber reinforcement's role in boosting ductility and elastic energy absorption. The disparity between peak strength displacement and maximum displacement suggests that post-peak toughness majorly contributes to overall toughness, with T_{150} impacting T_{total}. The highest T_{total} is observed in the M5R0 sample, and the lowest in M0R2.5, underscoring the importance of fiber content.

Upon examining the flexural stress-deflection curves in Fig. 11 (a), increasing fiber content in single-MSF samples enhances both the modulus of elasticity in the pre-peak zone and the displacement at peak strength, with M5R0 showing a higher displacement at peak than M2.5R0, indicating improved energy absorption. The M5R0's curve's gradual descent in the post-peak zone, notably sustaining high flexural stresses up to 2 mm of deflection, underlines its superior toughness, evidenced by its ability to withstand more displacement before failure, compared to the M2.5R0 sample. This demonstrates that greater fiber content significantly impacts post-peak toughness and ductility in single-MSF mixes. Fig. 12 illustrates a distinctive pattern in samples using manufactured steel fibers, marked by minor fluctuations throughout the curve. This behavior, attributable to the unique geometry of manufactured fibers, involves a cycle of fiber pullout and interlocking, affecting the sample's strength and deflection dynamics. To be detailed, the minor declines are attributed to the fiber pullout in its straight length, while minor rises are associated with fiber interlocking via its hooked ends.

Fig 11 (b) reveals that single-RSF samples display comparable elasticity before peak strength, with M0R5 peaking at a lower displacement and exhibiting a less pronounced decline after the peak, leading to greater T_{150} and T_{post} values. Both types of samples ultimately rupture at about 7 mm displacement, but single-RSF specimens demonstrate steadier stress curves with fewer abrupt changes, suggesting a stronger bond and better pullout resistance with the concrete matrix compared to manufactured fibers. Fig 11 (c) shows that hybrid samples share the same elasticity and peak strengths. The M2.5R2.5 sample, however, with its higher fiber content, experiences a smoother decline post-peak, indicating that increased fiber content in hybrid samples correlates with improved post-peak performance. Generally, higher fiber content correlates with increased toughness and flexural ductility, enhancing post-peak energy absorption, delaying crack initiation, and improving peak strength, which contributes to structural durability.

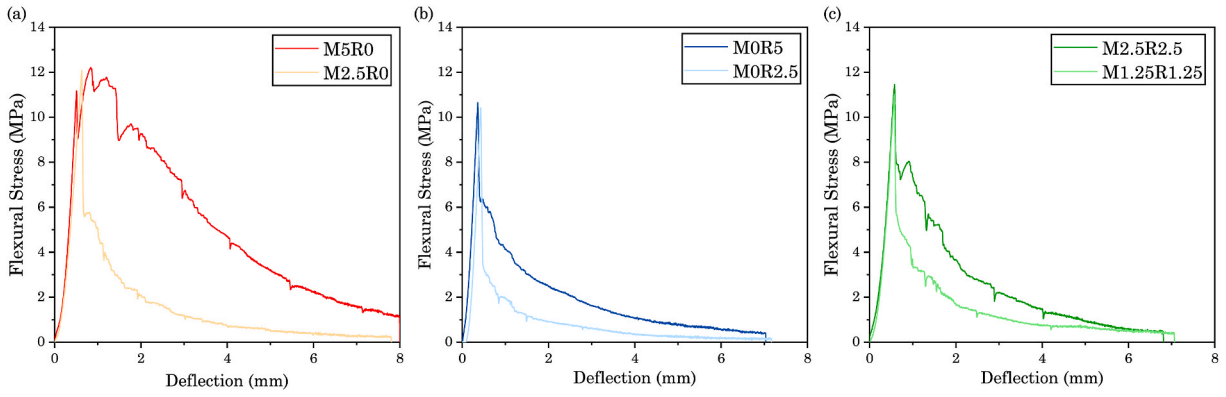

Fig. 11. Flexural behavioral curves of (a) single-MSF, (b) single-RSF samples, (c) hybrid.

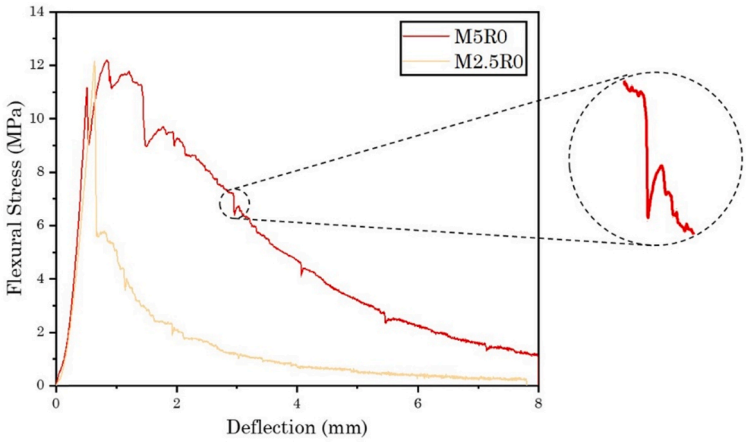

Fig. 12. Cycle of fiber pull out and interlocking in manufactured steel fibers.

3.1.4. Hybridization effect on flexural ductility

Fig. 13 contains a flexural behavioral curve of samples utilizing (a) 0.25 % vf fiber content, and (b) 0.5 % vf fiber content. Fig. 13 indicates that hybrid specimens typically fall between single-MSF and single-RSF samples in terms of flexural ductility. However, the M2.5R2.5 hybrid, with higher fiber content, aligns more closely with the M0R5 sample, while the M1.25R1.25 hybrid resembles the M2.5R0. This is evident from Fig. 10, where the toughness values of M2.5R2.5 are closer to M0R5, and those of M1.25R1.25 mirror M2.5R0.

In the low-fiber group of samples, the hybrid M1.25R1.25 sample exhibits higher stiffness in the elastic zone than the M2.5R0, as demonstrated in Fig. 13 (a), with the M0R2.5 showing the highest rigidity of all. The hybrid's enhanced stiffness is attributed to the combination of manufactured and recycled fibers, mostly because of the presence of RSFs. M1.25R1.25 also achieves peak strength at a larger deflection of 0.575 mm due to the utilization of manufactured fibers, enhancing ductility. Post-peak, M1.25R1.25's strength drop is less severe, closely resembling M2.5R0's pattern, indicating sustained flexural strength in the plastic zone through hybridization. The hybrid M1.25R1.25 sample also exhibits the characteristic minor fluctuations seen in manufactured fibers, underscoring the influence of these fibers on their post-peak flexural behavior. This mix effectively combines the best aspects of both fiber types, emerging as an optimal choice among low-fiber mixes.

The hybrid mix with 0.5 % vf fiber content showcases improved elastic stiffness and peak deflection compared to the single-RSF sample, a hallmark of the hybrid approach, as seen in Fig. 13 (b). This mix also displays the characteristic fluctuations associated with manufactured fibers. Compared to the M0R5 sample, the hybrid's curve drops less sharply, yet it doesn't closely resemble the M5R0 curve, which reminds the crucial effect of manufactured fibers in mixes with higher fiber contents. Instead, at higher deflections, it aligns more with M0R5, diverging from the pattern seen in lower fiber content hybrids. Essentially, the high-fiber hybrid sample mirrors single-RSF behavior more than the low-fiber group, where it closely matches the M2.5R0 sample.

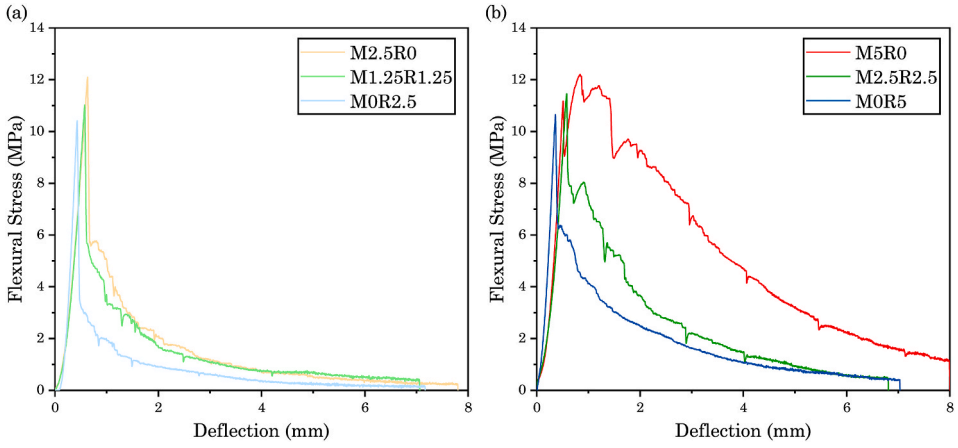

Fig. 13. Flexural behavioral curve of samples utilizing (a) 0.25 % vf fiber content, (b) 0.5 % vf fiber content.

3.2. Evaluation of surface damage index and crack patterns in FRC using DIC

Digital Image Correlation offers insights into crack development, indicating internal crack progression, using only the appeared cracks on the surface of the sample. Crack pattern analysis sheds light on stress distribution within structural elements, while the reinforcement in FRC influences crack growth and patterns. In this section, we evaluate the surface damage index and crack patterns to assess surface damage and characterize crack features in FRC. The surface damage index for each image is determined by calculating

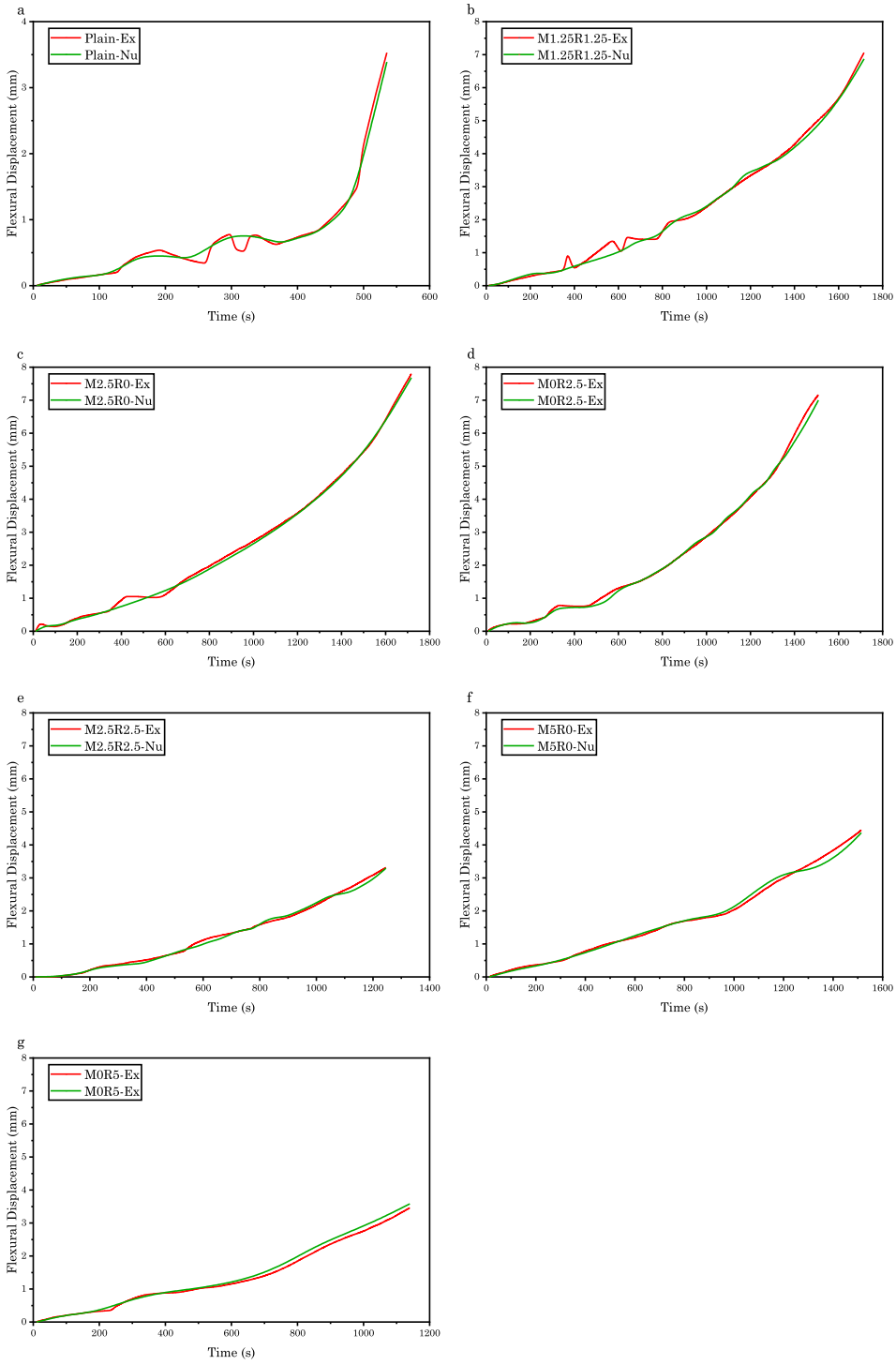

Fig. 14. DIC verification graphs for (a) Plain, (b) M1.25R1.25, (c) M2.5R0, (d) M0R2.5, (e) M2.5R2.5, (f) M5R0, (g) M0R5 samples.

the ratio of the damaged zone's area to the total area of the specimen. The DIC's color scale highlights horizontal displacement in millimetres, with blue indicating minimal damage and brown the most.

3.2.1. Verification of DIC with experimental result

The accuracy and dependability of Digital Image Correlation data were rigorously confirmed by comparing numerical results with experimental measurements. This validation process was crucial to ensure the reliability of the DIC method, which involved a thorough comparison across all mix designs. High congruence between DIC data and experimental results is illustrated in Fig. 14, which features seven groups of graphs. Each group represents a flexural (F) test for a particular mix, juxtaposing laboratory experimental outcomes (Ex) with DIC numerical analysis (Nu).

The verification process rigorously assessed the accuracy of DIC analysis by comparing it with experimental strain measurements for compressive tests and traditional methods for crack patterns. High-resolution DIC images of crack propagation in FRC specimens were validated against standard measurements, confirming DIC's reliability. Statistical analysis showed strong correlations and minimal discrepancies between DIC data and experimental results, establishing a trustworthy basis for interpreting the mechanical properties of fiber-reinforced concrete. This validation enhances the study's credibility and underscores DIC's efficacy in evaluating concrete's mechanical behavior.

3.2.2. Flexural surface damage index and observed crack pattern

Fig. 15 displays a series of eight DIC-analyzed images for each of the seven specimens, by employing MATLAB software, depicting the progression of crack development. These images are taken at specific deflections for all samples, except for stages (b) and (h), which correspond to the moments of peak strength and ultimate strength, respectively. Fig. 16 complements this by correlating the DIC analysis with the flexural stress-deflection curve for the M2.5R0 sample, providing a detailed visual narrative of crack formation and growth during the three-point bending test.

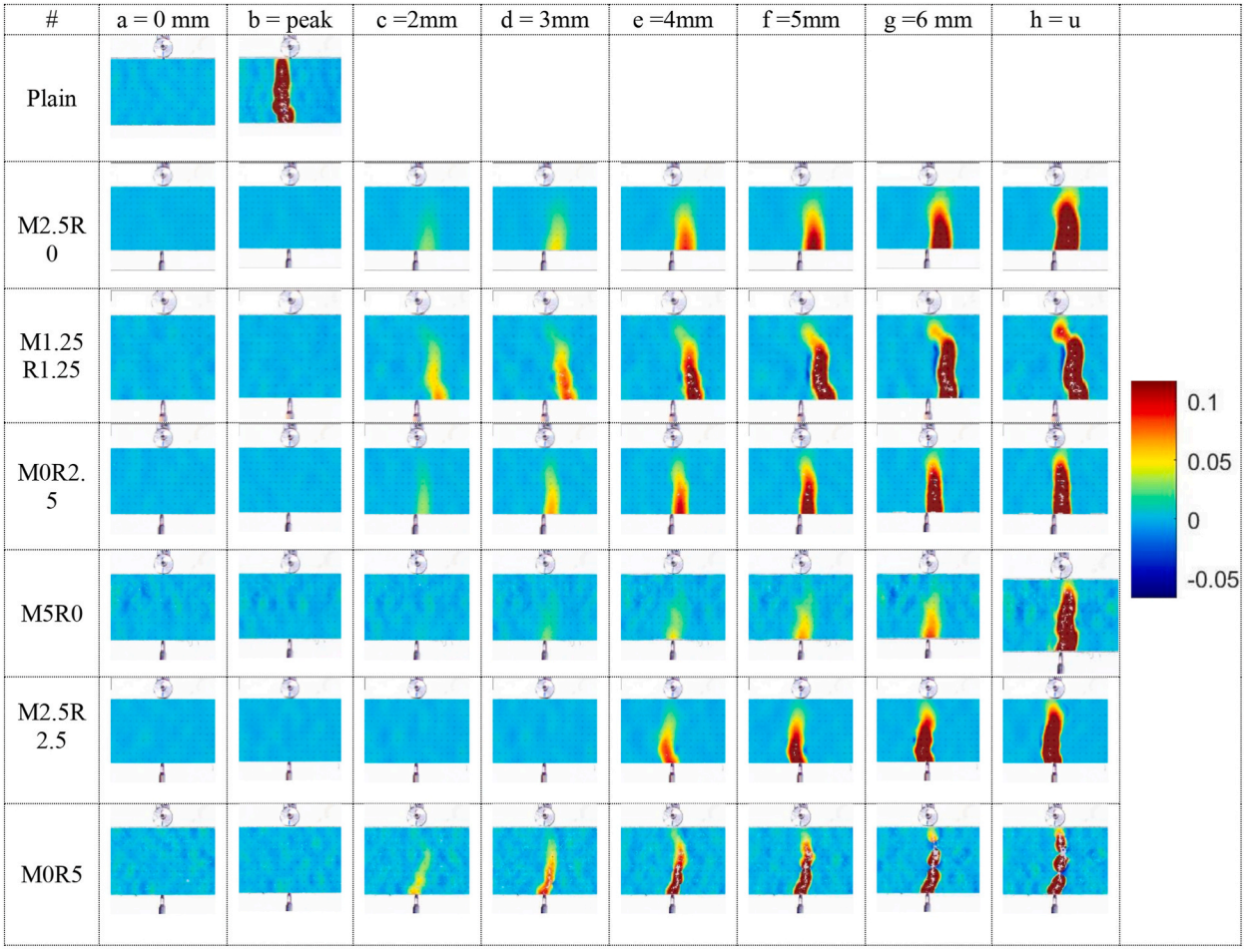

Fig. 15. DIC analysis of flexural samples.

DIC analysis reveals a delay when compared to flexural stress-deflection curves, with initial pictures showing no surface damage despite ASTM C 1609 indicating crack initiation at a deflection of L/600 (0.5 mm). This discrepancy is because DIC can only detect surface cracks, while actual crack initiation starts within the specimen. Thus, surface cracks visible in DIC images only appear after internal cracks have developed, leading to apparent delays in DIC's crack detection.

Compared to the plain specimen, FRC samples exhibit delayed crack initiation, as seen in Fig. 15. The plain sample fractures at a mere 0.2 mm deflection, indicative of a brittle failure, while FRC samples show no surface damage at this stage due to fiber reinforcement, leading to a more ductile failure. DIC analysis highlights the effects of fiber reinforcement, with fiber bridging visible in yellow during (c) to (f) stages, aiding in resisting crack propagation. Brown areas within the images denote areas where fibers have either failed as a result of pullout or rupture or are actively preventing crack growth. The properties of fiber reinforcement, including the fiber content and the reinforcement approach, influence the features of the cracks observed.

3.2.2.1. Fiber content effect on flexural SDI and crack pattern. Based on Fig. 16, in samples with only manufactured steel fibers, the M5R0 specimen shows a delayed crack initiation compared to M2.5R0, with the former initiating cracks at a later stage. DIC analysis reveals that, at any point, M5R0 exhibits smaller crack dimensions than M2.5R0. Moreover, despite achieving greater ultimate deflection, M5R0's maximum crack width in stage (h) is less than that of M2.5R0. Both samples exhibit flexural cracking aligned with the load direction, underscoring the impact of fiber reinforcement on crack development. Similar observations apply to hybrid samples, where the M2.5R2.5 specimen remains undamaged up to a 3 mm deflection, whereas the M1.25R1.25 starts showing surface crack propagation by this deflection. The specimen with higher fiber content consistently exhibits less severe crack widths throughout. Both display flexural-shear cracking patterns, with portions of the main crack inclined relative to the load direction. Fig. 17 showcases SDI curves for (a) single-MSF, (b) single-RSF, and (c) hybrid samples from DIC analysis. Notably, the SDI for the M2.5R0 sample spikes after 2 mm displacement, indicating the post-peak zone, while the M5R0 sample shows a more moderate SDI increase. Since a higher SDI implies larger cracks at the flexural sample's mid-span, the increased fiber content in single-MSF samples results in more controlled crack growth.

In single-RSF samples, crack initiation for both occurs at a 2 mm deflection. M0R5 has a narrower ultimate crack width but initially higher surface damage, which stabilizes, leading to a lower final SDI compared to M0R2.5. Despite similar SDI values up to 2.5 mm displacement, the higher fiber content in M0R5 slows SDI increase, suggesting controlled crack propagation due to more fibers at the crack's mid-span. Fig. 17 (c) demonstrates that the M2.5R2.5 samples exhibit minimal crack progression up to a 3 mm deflection. Echoing the behavior of single-MSF samples, the increased fiber content in these hybrids restricts crack development, enhancing the specimen's energy absorption capacity. Essentially, the crack propagation in M2.5R2.5 is notably postponed, with its SDI curve appearing as a delayed version compared to the M1.25R1.25 sample. Overall, the results suggest that higher fiber content generally reduces SDI but does not explore effects beyond the tested range.

3.2.2.2. Hybridization effect on flexural SDI and crack pattern. The advantages of hybridization are evident across M2.5R0, M1.25R1.25, and M0R2.5 samples. Adding recycled fibers to the mix narrows the ultimate crack width compared to M2.5R0, and hybrid samples exhibit shorter cracks than both groups of low-fiber and high-fiber. The influence of manufactured fibers is particularly notable. Fig. 18 shows that areas with manufactured fibers display a larger yellow zone atop the brown cracked surface, indicating

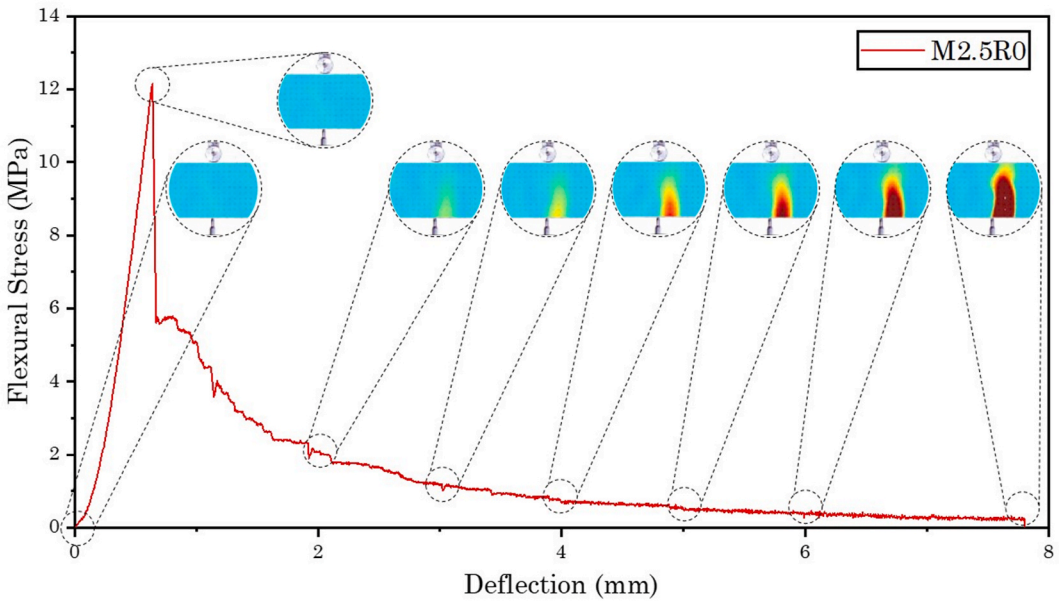

Fig. 16. DIC analysis alongside the load-deflection curve of the M2.5R0 sample.

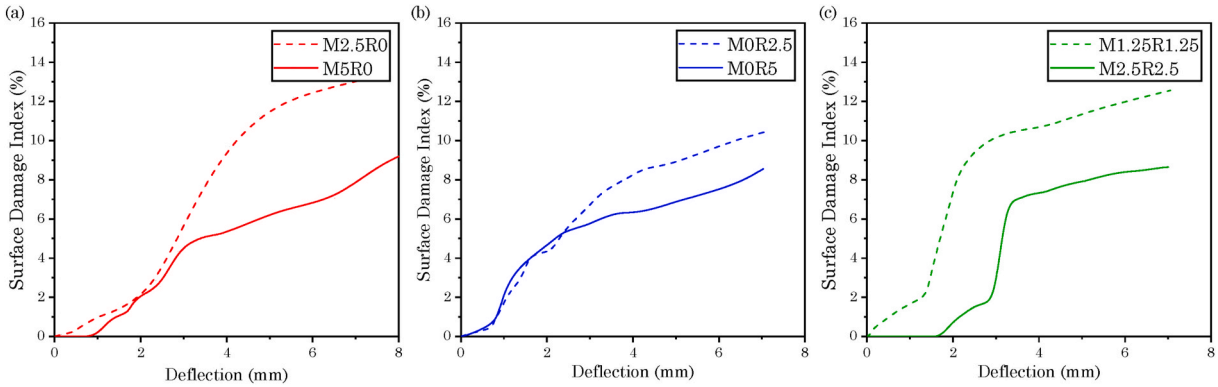

Fig. 17. Surface damage index curves for (a) single-MSF, (b) single-RSF, (c) hybrid samples.

these fibers' role in halting crack surface spread. This effect, attributed to the double-hooked design of manufactured fibers interlocking with the concrete, helps preserve the height of the cross section's uncracked zone, thereby maintaining the flexural strength of the uncracked section. This result aligns with experimental findings, which highlight the strong potential of MSFs to bridge wide cracks in the post-peak zone.

The impact of manufactured fibers is also seen in the hybrid sample, where a significant yellow zone above the damaged area highlights MSF interlocking, reducing the main crack length compared to low-fiber single-fiber samples. This maintains flexural resistance more effectively.

The difference in crack width between the M0R2.5 and M2.5R0 samples is pronounced, with narrower cracks in the single-RSF sample. This variation stems from the earlier noted flexural behavior analysis: manufactured fibers form weaker bonds with the concrete matrix along their straight length compared to recycled fibers. Consequently, single-MSF samples exhibit a binary crack width pattern—either minimal or at least the size of fibers' straight length. In contrast, recycled fiber samples demonstrate gradual crack widening due to stronger fiber-concrete bonding, resulting in consistently narrower crack widths even at peak strength deflections. Fig. 19 shows SDI curves from DIC analysis for (a) low-fiber, and (b) high-fiber samples, highlighting how each fiber type influences SDI trends. M2.5R0's SDI surges due to its two-stage flexural behavior linked to MSF characteristics. Conversely, M0R2.5's SDI gradually increases, aligning with RSF's effective stress distribution, confirming its greater bond with concrete.

The initially puzzling high SDI of the M1.25R1.25 sample, as per Fig. 15 step (h), aligns with the understanding that a greater SDI reflects broader stress distribution, as indicated by the yellow zone common to single-MSF samples. This suggests the positive influence of manufactured fibers, though a 0.125 % vf content of each fiber type may not fully capture their collaborative potential. For high-fiber samples, early crack initiation in M0R5 contrasts with M5R0's later onset at around 3 mm deflection. The hybrid M2.5R2.5 benefits from M5R0's characteristics, displaying improved energy absorption and narrower cracks, underscoring the hybrid advantage in managing stress and cracks. In the M0R5, consistent crack widths in the final stages point to stable crack growth and even stress distribution. The M5R0, however, shows increases in crack size throughout testing, a trend also present in low-fiber samples. The M2.5R2.5 maintains stable crack widths, indicating balanced flexural-shear strength. Fig. 19 (b) exhibits the combined RSF and MSF effects in the M2.5R2.5, with minimal damage until a 3 mm deflection and better integrity preservation than single-fiber samples, making it a favorable choice for reducing surface cracks under typical loads.

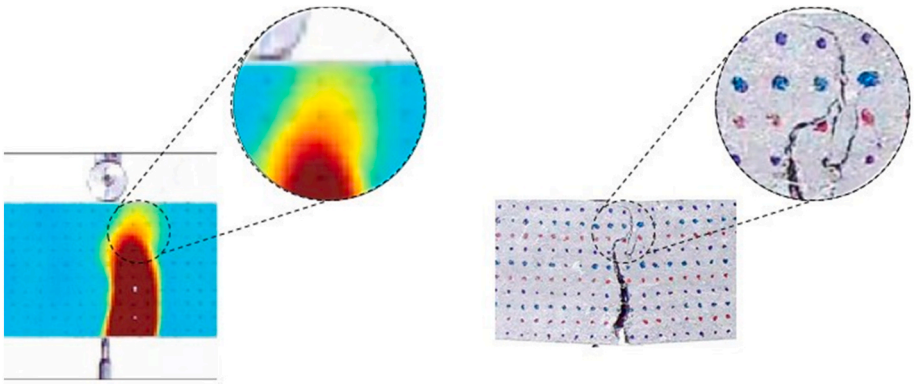

Fig. 18. Top layer of the brown-colored cracked area in M2.5R0 flexural sample. (For interpretation of the references to color in this figure legend, the reader is referred to the Web version of this article.)

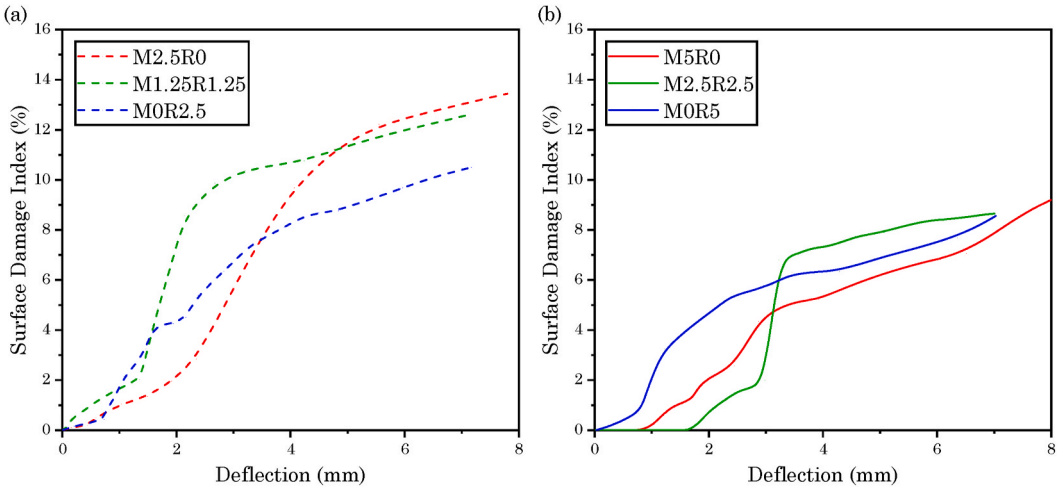

Fig. 19. Surface damage index curves for flexural samples utilizing (a) low-fiber, (b) high-fiber samples.

3.3. Evaluation of fiber reinforcement efficiency using CT-scan

The findings from the CT-scan analysis are divided into two sections. The first section evaluates the impact of fiber content, while the second section discusses the effect of hybridization in fiber reinforcement, and both assess the observed failure state of FRC samples. Initial results are derived from CT-scan images, with additional consideration given to data extracted from fibers affected by the primary crack. Utilizing the Avizo, the count of recycled and manufactured fibers affected by the primary crack in all six FRC samples is calculated. These fibers are categorized into three groups: "Ruptured," "Pulled-out," and "Bridging," based on their observed condition in the final stage of each sample. Specifically, the Avizo software detects each fiber piece, after which the authors classify fibers as bridging, pulled-out, or ruptured, one by one. Bridging fibers are intact and hooked on both sides of the main crack. Pulled-out fibers are intact, hooked at one end but pulled out of the concrete body on the other end. The rest are ruptured fibers, which are identified by their pieces, typically broken into two; therefore, the number of pieces divided by two equals the number of ruptured fibers. Table 8 presents these data alongside the percentage of each group, while this data is depicted in Fig. 20.

3.3.1. Fiber content effect on microstructural interaction

Data obtained from CT-scans, along with information from Table 8 and Fig. 20, indicate that increasing the fiber content from 0.25 % vf to 0.5%vf in single-MSF samples, while enhancing mechanical and flexural characteristics to a certain degree, results in the fiber reinforcement performing less efficiently. Fig. 21 presents 3D CT-scan images of all Fiber-Reinforced Concrete samples. Upon initial examination, it is apparent that in samples with a higher fiber content, about twice the number of fibers is involved in interacting with the primary flexural crack compared to the samples with a lower fiber content.

Upon closer examination, it becomes evident that in single-MSF samples, an increase in fiber content leads to a diminished efficiency in the microstructural performance of the manufactured fibers. Specifically, Fig. 20 highlights that the M5R0 sample exhibits a 17 % increase in the proportion of pulled-out fibers compared to the M2.5R0 sample, resulting in a nearly 15 % decrease in the proportion of ruptured fibers. Fig. 22 offers a 2D depiction of this phenomenon, where a significant number of manufactured fibers in the M5R0 sample are shown to be pulled out. Furthermore, Table 8 reveals that among the 151 additional primary crack-affected MSFs

Table 8
Count and percentage of fibers affected by the main crack, grouped by their observed condition.

	Mix Design	MSF				RSF			
		Ruptured	Pulled-out	Bridging	Sum	Ruptured	Pulled-out	Bridging	Sum
Number of fibers	M2.5R0	46	37	35	118	0	0	0	0
	M1.25R1.25	35	20	24	79	57	17	20	94
	M0R2.5	0	0	0	0	68	26	35	129
	M5R0	65	131	73	269	0	0	0	0
	M2.5R2.5	61	30	39	130	91	22	29	142
	M0R5	0	0	0	0	174	65	96	335
Percentage of fibers	M2.5R0	38.98	31.36	29.66	100	–	–	–	–
	M1.25R1.25	44.30	25.32	30.38	100	60.64	18.09	21.28	100
	M0R2.5	–	–	–	–	52.71	20.16	27.13	100
	M5R0	24.16	48.70	27.14	100	–	–	–	–
	M2.5R2.5	46.92	23.08	30.00	100	64.08	15.49	20.42	100
	M0R5	–	–	–	–	51.94	19.40	28.66	100

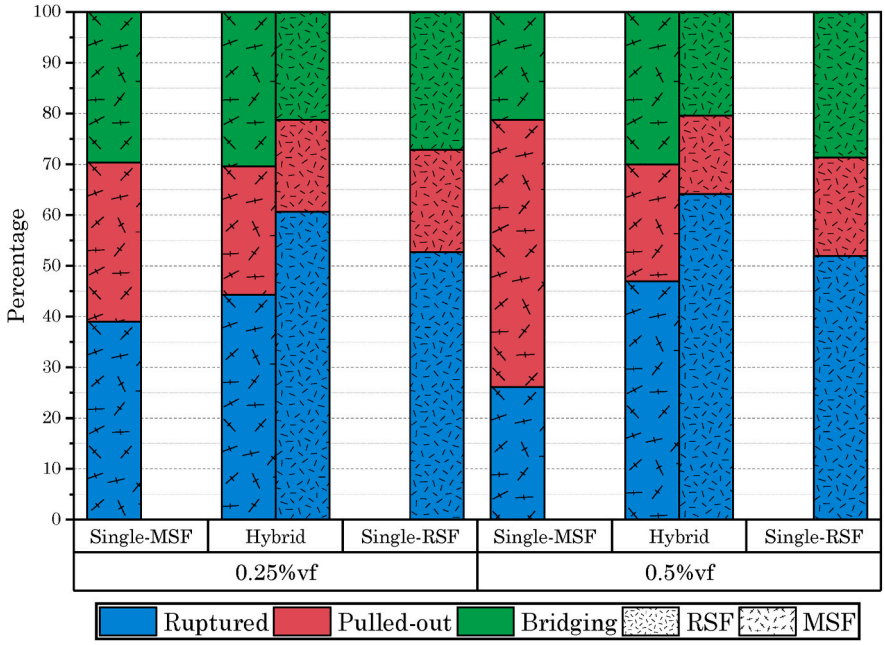

Fig. 20. Percentage of fibers affected by the main crack, grouped by their observed condition.

present in the M5R0 sample relative to the M2.5R0, only 19 undergo rupture, whereas 94 experience pullout failure. This suggests that the single-fiber reinforcement approach may not be the most efficient strategy at higher MSF fiber content. To enhance the performance, the concrete matrix requires a stronger bond with the manufactured fibers, mitigating the likelihood of fiber pullout.

When examining single-RSF samples, the data indicates negligible differences in fiber reinforcement efficiency between the low and high-volume fractions of recycled fiber samples. Fig. 20 illustrates that the ratios of ruptured and pulled-out fibers at the ultimate failure stage of these samples are nearly identical, demonstrating that a higher fiber content does not individually influence fiber performance. Moreover, the hybrid analyses, as depicted in Fig. 20, reveal a modest uptick in the percentage of ruptured fibers accompanied by a minor reduction in the incidence of fiber pullout. This trend is consistent across different fiber types, suggesting that the performance enhancement is a consequence of increased fiber content.

3.3.2. Hybridization effect on microstructural interaction

Evidence derived from CT scans and data from Table 8 strongly supports the positive effects of hybridization in fiber reinforcement. These findings primarily emphasize the role of recycled steel fibers in the enhancement of integrity and ductility in concrete as a result of the closure of numerous micro-cracks, leading to more efficient performance of manufactured fibers. Additionally, they underscore the responsibility of MSF in bridging the main crack, further solidifying the benefits of hybridization in fiber reinforcement.

3.3.2.1. Hybridization effect on MSF failure mechanism. Fig. 20 shows that in the M2.5R0 sample, only 39 % of the manufactured fibers affected by the primary crack ruptured. This situation worsens in the M5R0 sample, where the rate of fiber rupture drops to 24 %, with twice as many fibers experiencing pullout instead. However, the scenario improves with hybrid samples, where at least 44 % of all manufactured fibers end up rupturing by the final stage, reducing the pullout rate to 25 % or even less. Moreover, the presence of bridging fibers slightly increases. For instance, the M2.5R2.5 sample has a similar count of affected manufactured synthetic fibers (MSFs) as the M2.5R0, but the addition of just 0.25 % volume fraction (vf) of recycled fibers results in nearly a 5 % boost in the rate of fiber rupture and about a 6 % drop in the rate of fiber pullout. Fig. 23 further visualizes these findings, highlighting that in the M5R0 sample, a majority of fibers rupture, whereas, in the M2.5R2.5 sample, the fibers are mainly pulled out. This comparison simplifies understanding by illustrating the impact of hybridization on the efficiency of fiber reinforcement in concrete.

The higher rate of ruptured fibers directly signifies the maximum utilization of fiber load capacity, indicating that hybridization in FRC samples has resulted in greater efficiency of fiber performance. In simpler terms, the presence of recycled fibers has fostered an enhanced environment for manufactured fibers to perform optimally. This section substantiates the observation of narrower crack widths in the M2.5R2.5 sample as identified through DIC analysis, as an effect of hybridization.

3.3.2.2. Hybridization effect on MSF bonding with concrete. Despite the intention behind adding hooked ends to steel fibers to strengthen their bond with concrete matrix, the bond often proves weaker than the fibers' tensile strength, which is spotted to be a leading cause of frequent manufactured fiber pullout. This situation often arises when the surrounding concrete matrix weakens due to extensive flexural loading and associated internal forces. In some cases, even the bonding strength of undamaged concrete is lower

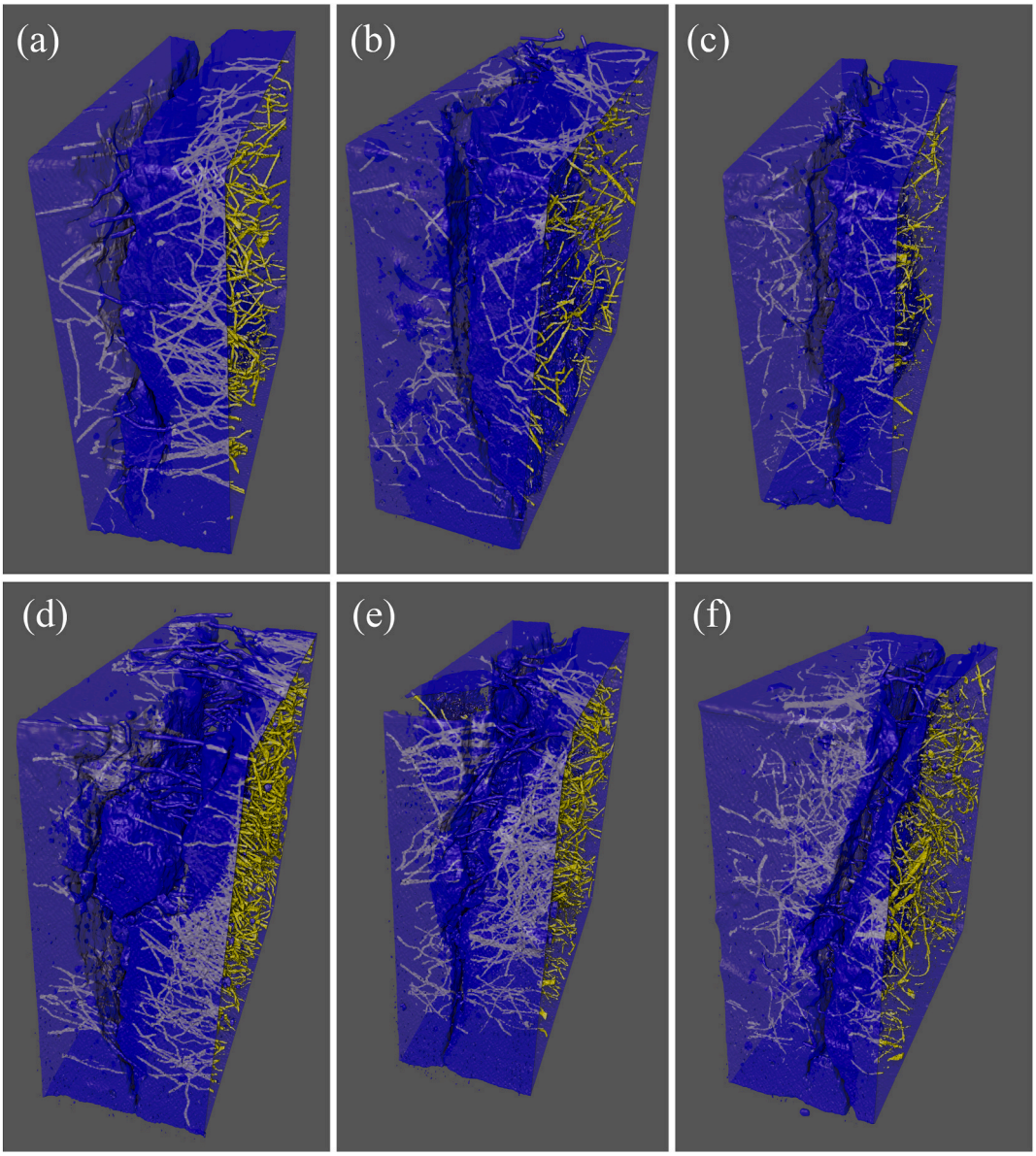

Fig. 21. 3D CT-scan images of M2.5R0 (a), M1.25R1.25 (b), M0R2.5 (c), M5R0 (d), M2.5R2.5 (e), and M0R5 (f) samples.

than the tensile strength of the fiber. As illustrated in Fig. 24 (a), recycled fibers located near manufactured fibers can reduce the extent of damage to the nearby concrete matrix or keep it undamaged. In contrast, in the single-MSF sample depicted in Fig. 24 (b), manufactured fibers affected by the main crack cause damage to the surrounding concrete in the form of additional air voids or micro-cracks near the hooked ends.

The repercussions of this incident become evident when comparing the percentage of ruptured manufactured fibers between single-MSF and hybrid specimens. The enhanced bonding strength resulting from the inclusion of recycled steel fibers causes more fibers to fail due to rupture rather than pullout. This section provides evidence for the delayed rise in the SDI parameter observed in the M2.5R2.5 sample during the DIC analysis. Also, it confirms the RSF potential in pre-peak rigidity,as it prevents micro cracks.

3.3.2.3. Hybridization effect on crack pattern. The observed crack patterns in both single-fiber and hybrid samples also highlight the advantageous effects of hybridization. As depicted in Fig. 25 (a), no additional micro-cracks are formed in the vicinity of the primary crack. However, in Fig. 25 (b), additional micro-cracks form and propagate alongside the main flexural crack in the single-MSF sample.

This statement further underscores the crucial role of recycled steel fibers in controlling microcracks in vulnerable areas of concrete. By preventing the formation of microcracks, RSFs help maintain the integrity and unity of the concrete matrix. This, in turn,

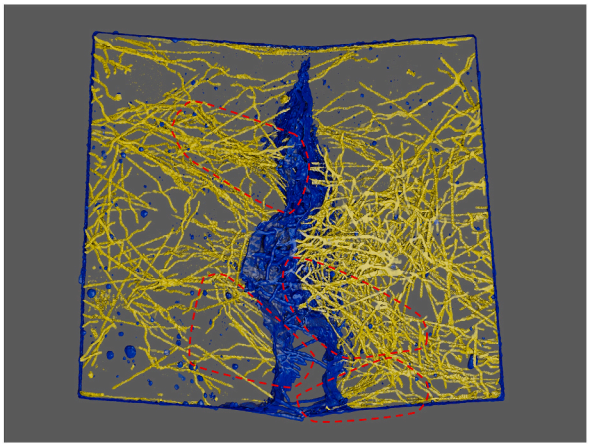

Fig. 22. Fiber pullout in large numbers in the M5R0 sample.

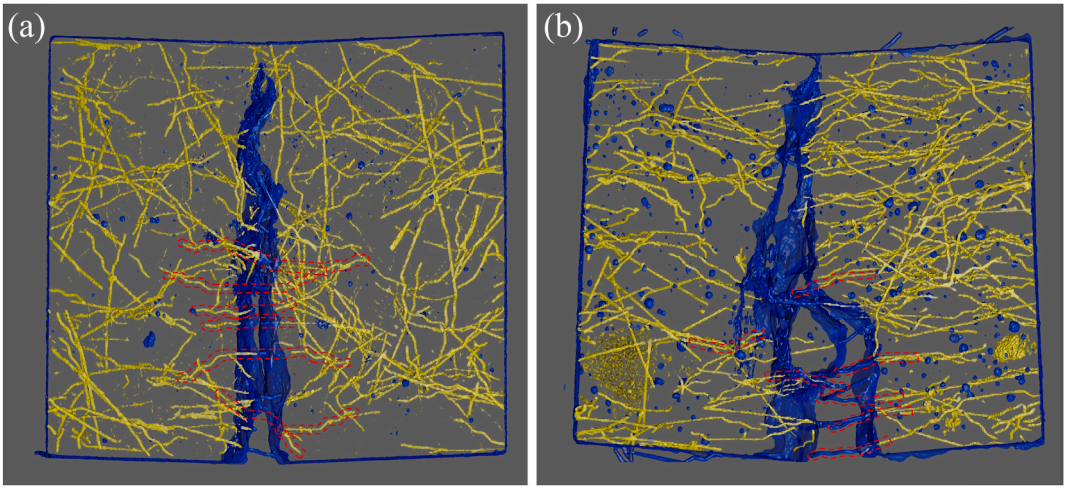

Fig. 23. Ruptured MSFs in M2.5R2.5 (a), and Pulled-out MSFs in M5R0 (b) samples.

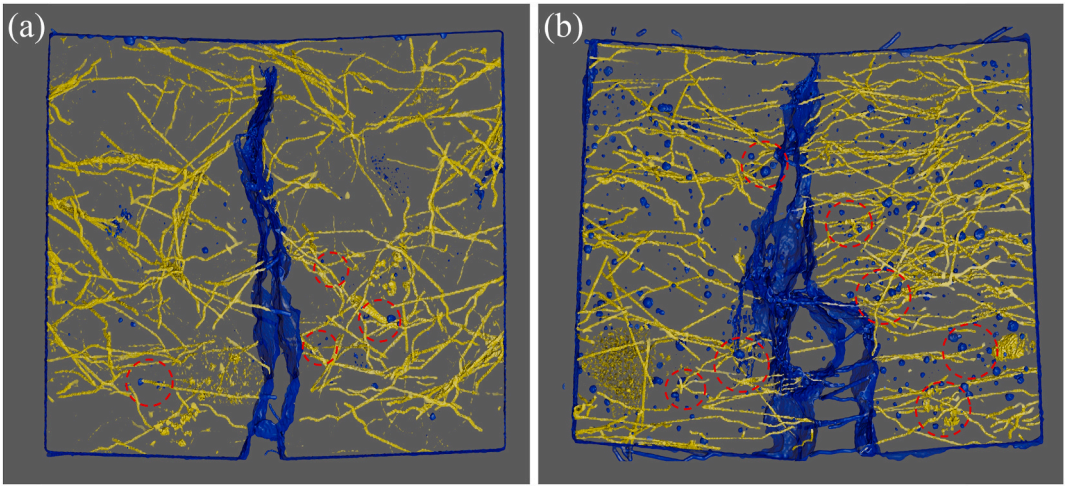

Fig. 24. The severity of concrete damage in M2.5R2.5 (a), and M5R0 (b) samples.

enhances the bonding strength between MSFs and the concrete matrix, ultimately leading to higher efficiency in the performance of steel fibers.

3.3.2.4. Primary role of RSF in microstructural performance of FRC. The main motivation behind studying hybrid steel fiber mixtures in this paper is to assess the influence of RSFs in the FRC mixture. Previous studies have discussed how surface treatments applied to MSFs, along with their double hooked-ends, assist manufactured fibers in forming a stronger bond with the concrete matrix compared to recycled steel fibers. However, the data presented in Fig. 20 indicate that the majority of recycled fibers experience rupture rather than pullout, regardless of the mixture and fiber content. This occurrence can be attributed to the irregular shape of recycled steel fibers utilized in this study, which are obtained from automobile waste tires, within the concrete matrix. For example, in Fig. 26 ruptured and bridging recycled fibers in the M5R0 (a) and M2.5R2.5 (b) sample are highlighted by red and green borders, respectively.

RSFs do not necessarily assume a straight position within the concrete; instead, they often adopt a random irregular shape. This unpredictable shape can result in bends and curves along their length, effectively acting as hooks. These incidental hooks, coupled with the relatively thin nature of recycled fibers, often lead to a higher concrete-fiber bonding strength than steel tensile strength. Consequently, even in single-RSF samples, more than 50 % of all fibers in the primary crack area are ruptured, while less than 20 % are pulled out. In hybrid samples, the proportion of ruptured recycled fibers can be as high as 60 %. Moreover, it's important to note that beyond the aforementioned advantages, RSFs offer significant environmental and economic benefits when used in fiber-reinforced concrete.

3.4. Evaluation of fiber-concrete boding using SEM

3.4.1. Fiber Interface Transition Zone (FITZ)

The Fiber Interface Transition Zone (FITZ) is a crucial area (~30 μm of fiber) in FRC where fibers interact with the matrix material [61] as illustrated in Fig. 27. Its unique properties distinguish it from the surrounding bulk concrete and the fibers themselves. The FITZ's characteristics and behaviors significantly influence the overall performance of fiber-reinforced concrete. The interaction of fibers with the surrounding matrix is crucial for improving the structural design and performance of FRC. The FITZ is characterized by concrete-fiber detachment, which occurs between the concrete matrix and the imbedded fibers. This detachment can occur throughout the fibers, indicating a breakdown in the connection between the concrete and the fibers. The interaction of fibers with the surrounding matrix is essential for enhancing the performance of fiber reinforced concrete. Separation of concrete and fibers in the FITZ can occur due to stress concentrations, differential properties, and fiber pull-out. Detachment can be observed as fissures or holes between individual fibers and the concrete matrix. Scanning electron microscopy images show cracks near steel fibers, indicating the weakening of bonding links. The separation of concrete fibers in the FRC of the FITZ can affect the material's performance and durability. The load transfer mechanism between fibers and the matrix may be compromised, reducing fiber reinforcement efficacy. Disconnected fibers may also allow moisture to penetrate the material, resulting in deterioration and reduced durability.

3.4.2. FITZ analysis in single-fiber mix approach

SEM images from single-fiber samples reveal key differences in crack behavior between single-MSF and single-RSF specimens, as shown in Fig. 28. These differences largely stem from the use of double-hooked ends in MSFs, which significantly improve fiber-concrete bonding and interlocking, thereby enhancing crack bridging efficiency. The production of MSFs often includes surface treatments, such as double hooking, to improve fiber-matrix interaction, facilitating better stress distribution and reducing crack

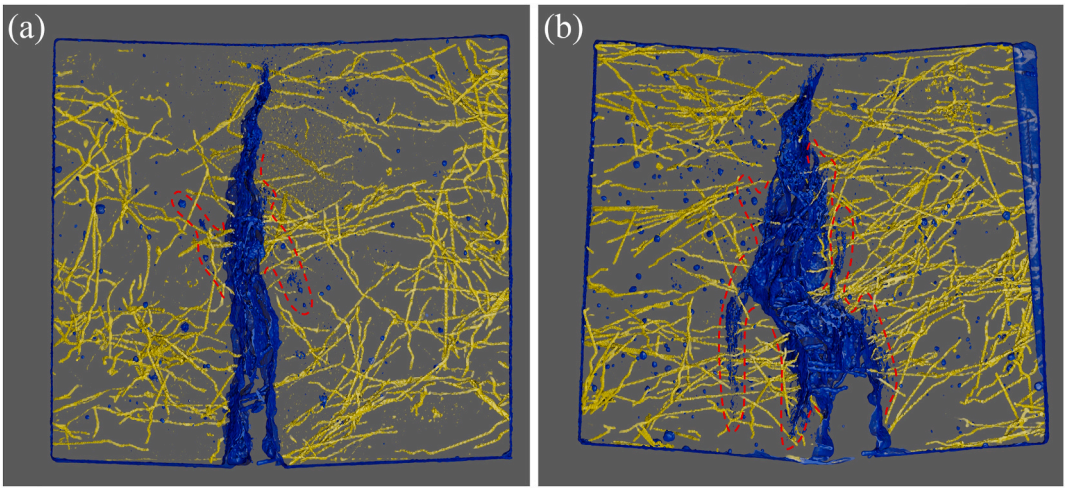

Fig. 25. The formation of additional micro-cracks in M2.5R2.5 (a), and M5R0 (b) samples.

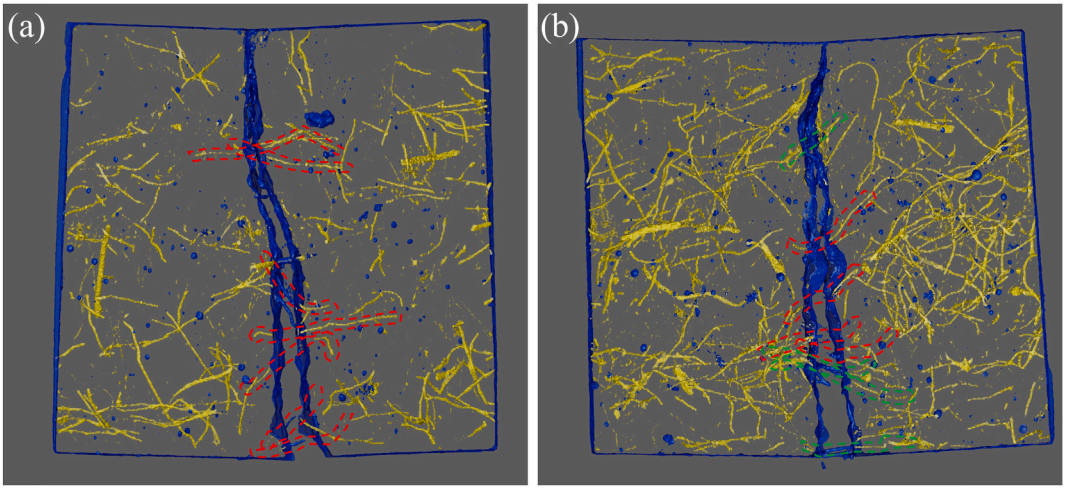

Fig. 26. Ruptured and bridging RSFs in M0R2.5 (a), and M2.5R2.5 (b) samples.

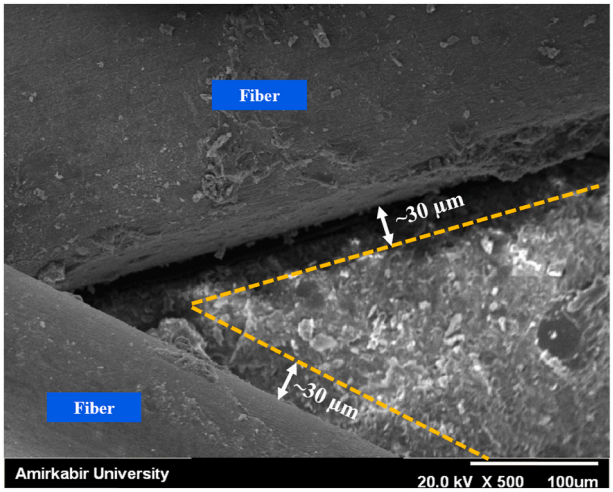

Fig. 27. The fiber interface transition zone.

depth. The geometry of MSFs, especially their hooked ends, promotes effective mechanical interlocking and crack deflection, resulting in shallower cracks, as its clear in Fig. 28 (a).

Conversely, single-RSF samples exhibit deeper cracks, depicted in Fig. 28 (b), likely due to the absence of surface treatments and the variable severity of crack depth caused by their irregular shapes. However, the higher crack depth does not necessarily mean a higher fiber pullout rate, as recycled fibers can obtain any random physical shape and consequently avoid pullout. Thus, when employing a single-fiber strategy, manufactured steel fibers demonstrate superior crack-resistant properties compared to recycled steel fibers.

3.4.3. FITZ analysis in hybrid-fiber mix approach

Despite the enhanced bonding strength from double-hooked ends and surface treatments on manufactured steel fibers, CT-scan data reveal frequent pullouts in the M2.5R0 sample, worsening in the M5R0 sample with a pullout rate of nearly 49 %. This indicates the need for strategies to further boost the fiber-concrete bond. Fig. 29 illustrates the crack depth and extent of fiber detachment in both M2.5R0 and M2.5R2.5 samples.

A side-by-side analysis of Fig. 29 (a) and (b) shows that MSFs in the hybrid sample experience less detachment from the concrete compared to the single-MSF sample, highlighting the beneficial impact of adding 0.25 % vf recycled steel fibers on MSF-concrete bonding efficiency. Indeed, the twisted and randomly curved shapes of RSFs function like natural hooks, preventing the formation of microcracks in concrete and thereby facilitating improved stress distribution within the matrix. This observation aligns with CT-scan findings, showing that the hybridization approach leads to a 6 % decrease in MSF pullout for low-fiber mixes and an even more substantial 26 % reduction for high-fiber mixes. Thus, although RSFs may not directly improve primary crack bridging, they help prevent micro-crack formation, thereby strengthening the MSF-concrete bond and enhancing overall MSF and FRC performance.

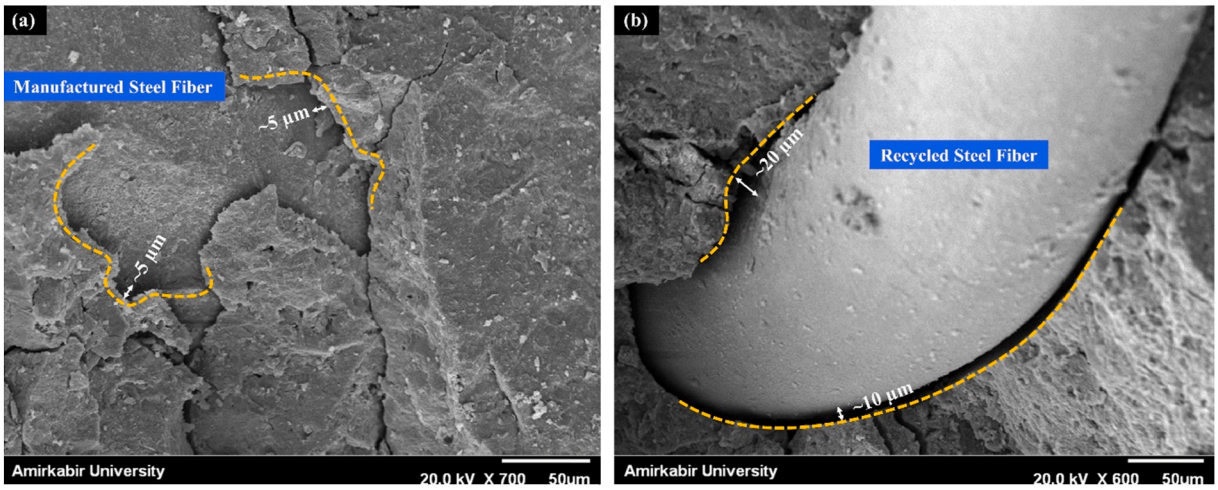

Fig. 28. Fiber separation from concrete in M5R0 (a), and M0R5 (b) samples.

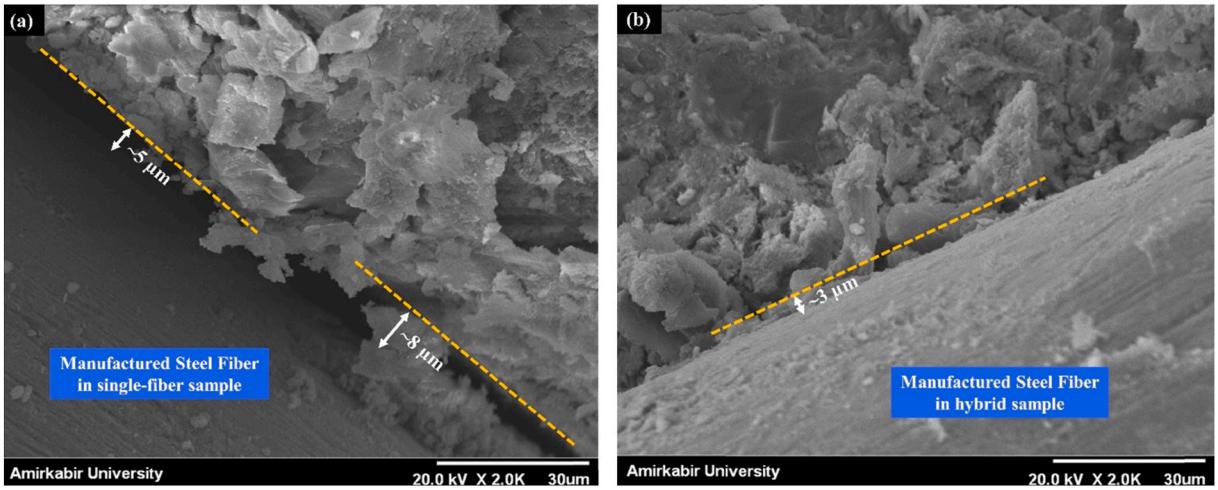

Fig. 29. Fiber separation from concrete in M2.5R0 (a), and M2.5R2.5 (b) samples.

4. Conclusion

This study offers an in-depth assessment of the flexural properties of Hybrid Fiber Reinforced Concrete, which incorporates both recycled steel fibers recovered from waste tires and manufactured steel fibers. The study utilizes a four-stage methodology to analyze fiber reinforced concrete with recycled and manufactured fibers. Techniques include experimental flexural loading tests, Digital Image Correlation, CT-Scan, and Scanning Electron Microscopy. These complementary stages assess the unique contributions of different fibers in enhancing the mechanical properties of concrete. The conclusive results are organized into three distinct sections. The first section analyzes the impact of fiber content on concrete's flexural performance, while the subsequent two sections examine the specific roles of each fiber type within hybrid fiber-reinforced mixtures.

Based on the findings of this study, the M2.5R2.5 mix appears to offer the most favorable balance of performance and efficiency. While the M5R0 mix demonstrates slightly higher flexural strength and ductility, the M2.5R2.5 mix achieves comparable results with more efficient fiber usage, as confirmed by the CT-scan and SEM analysis. Additionally, the use of 50 % recycled steel fibers in the M2.5R2.5 mix provides an added environmental advantage without compromising performance. Therefore, volume fractions of 0.25 % RSF and 0.25 % MSF can be declared as optimal dosage of fibers in this study.

Fiber content effect on flexural performance.

- Increased fiber content enhances toughness, ductility, and surface damage resistance.
- In single-MSF mixes, the improvements are most significant, while hybrid and single-RSF mixes show moderate yet effective results.

- While higher MSF content increases flexural strength, it reduces efficiency due to a higher tendency for fiber pull-out, highlighting the importance of optimizing fiber dosage.

Role of manufactured steel fibers in hybrid FRC.

- Similarly noted in single-MSF samples, manufactured steel fibers excel in delivering post-peak ductility and toughness, thanks to their strong capability to bridge large and primary flexural cracks.
- The capability of MSFs to bridge wider cracks enables the flexural sample to endure greater deflections while preserving its flexural strength.
- Despite being provided with surface treatment and equipped with double-hooked ends, the interlocking potential of MSFs is significantly influenced by the presence of nearby micro-cracks in the concrete matrix.

Role of recycled steel fibers in hybrid FRC.

- RSFs play a critical role in improving pre-peak rigidity by controlling micro-crack formation, which enhances the concrete matrix's integrity.
- The performance of MSFs in hybrid FRC is significantly enhanced by the inclusion of RSFs, which help control micro-cracks near the hooked ends of MSFs.
- The random and irregular shape of recycled steel fibers naturally forms curves that act like hooks, providing RSFs with an overall higher bonding strength to concrete compared to MSFs.

Hybridization effect on flexural performance.

- Hybrid mixes combining RSFs and MSFs show a more balanced improvement in flexural performance, with a stronger bond between fibers and the concrete matrix.
- The addition of recycled steel fibers to manufactured steel fibers, leads to an increased rate of MSF rupture and a decreased rate of pull-out, by nearly 23 % and 26 % respectively, fully unleashing the potential of MSFs and improving the flexural performance of the FRC.
- The addition of RSFs reduces crack width by lowering the rate of MSF pull-outs.
- The synergistic effect of MSFs and RSFs is particularly pronounced in the microstructure of FRC. While peak flexural strengths may not show significant variation across samples, the overall efficiency of fiber reinforcement is greatly enhanced.

Notably, this study has limitations. The CT-scan methodology could be improved with a real-time CT-scan device, allowing for continuous observation and analysis during pre-peak, peak, and post-peak stages. This enhancement, similar to the SDI evaluation, would enable detailed insights into the interaction between fibers and the concrete matrix, potentially leading to a deeper understanding of each fiber behavior and failure modes throughout the test.

CRediT authorship contribution statement

Tohid Asheghi Mehmandari: Writing – review & editing, Writing – original draft, Validation, Software, Methodology, Formal analysis, Data curation. **Mehdi Shokouhian:** Writing – review & editing, Writing – original draft, Software, Methodology. **Mohammad Zakeri Josheghan:** Writing – review & editing, Writing – original draft, Supervision, Conceptualization. **Seyed Ali Mirjafari:** Writing – review & editing, Writing – original draft. **Ahmad Fahimifar:** Writing – review & editing, Writing – original draft, Validation, Supervision, Conceptualization. **Danial Jahed Armaghani:** Writing – review & editing, Writing – original draft, Supervision, Conceptualization. **Kong Fah Tee:** Writing – review & editing, Writing – original draft, Supervision.

Declaration of competing interest

The authors declare that they have no known competing financial interests or personal relationships that could have appeared to influence the work reported in this paper.

Data availability

Data will be made available on request.

References

[1] S. Alrekabi, A. Cundy, A. Lampropoulos, R. Whitby, I. Savinas, Mechanical performance of novel cement-based composites prepared with nano-fibres, and hybrid nano-and micro-fibres, Composite Structures Name 178 (2017) 145–156.
[2] N. Roshan, M. Ghalehnovi, S.S. Pakzad, Recycled steel fiber for fiber reinforced concrete production: fresh and hardened properties, cost, and ecological assessments, Journal of Building Pathology and Rehabilitation 24 (2023).

[3] H. Nguyen, M. Staudacher, P. Kinnunen, V. Carvelli, M. Illikainen, Multi-fiber reinforced ettringite based composites from industrial side streams, J. Clean. Prod. 211 (2019) 1065–1077.
[4] F. Grzymski, M. Musial, T. Trapko, Mechanical properties of fibre reinforced concrete with recycled fibres, Constr. Build. Mater. 198 (2019) 323–331.
[5] M. Khormani, V.R.K. Jaaris, Statistical analysis of the compressive strength of concrete using 2D DIP technology and Finite Element Method, Case Studies in Construction Materials Name 19 (2023) e02461.
[6] J. McIntosh, K. Gharehbaghi, K.F. Tee, A. De Luca, J.S. Taylors, Viability rubric of fibre-reinforced polymer composites for civil infrastructure applications, Infrastructure Asset Management Name 40 (2023) 1–10.
[7] Zhiqiang Gu, et al., Effects of steel fibers on the flexural behavior of recycled concrete beam: testing and analysis, J. Build. Eng. 85 (2024) 108718.
[8] C. Frazao, B. Diaz, J. Barros, J.A. Bogas, F. Toptan, An experimental study on the corrosion susceptibility of recycled steel fiber reinforced concrete, Cement and Concrete Composites Name 96 (2019) 138–153.
[9] C. Frazão, J. Barros, A. Camões, A.C. Alves, L. Rocha, Corrosion effects on pullout behavior of hooked steel fibers in self-compacting concrete, Cem. Concr. Res. 79 (2016) 112–122.
[10] M. Mastali, A. Dalvand, A. Sattarifard, M. Illikainens, Development of eco-efficient and cost-effective reinforced self-consolidation concretes with hybrid industrial/recycled steel fibers, Construction and Building Materials Name 166 (2018) 214–226.
[11] N. Buratti, C. Mazzotti, M. Savoias, Post-cracking behaviour of steel and macro-synthetic fibre-reinforced concretes, Construction and building materials Name 25 (2011) 2713–2722.
[12] M Mastali, A Dalvand, Fresh and hardened properties of self-compacting concrete reinforced with hybrid recycled steel–polypropylene fiber, J. Mater. Civil Eng. 29 (6) (2017).
[13] M. Eskandarinia, M. Esmailzade, A. Hojatkashani, A. Rahmani, S. Jahandari, Optimized alkali-activated slag-based concrete reinforced with recycled tire steel fiber, Materials Name 15 (2022) 6623.
[14] F.M. Alharthi, M.A. Al-Osta, M.K. Rahman, A.A. Bahraq, S. Ahmad, M.M. Al-Zahrani, A. Elamarys, Flexural behavior of concrete hollow-core beams reinforced with GFRP bars: experimental and analytical investigation, Arabian Journal for Science and Engineering Name 49 (2024) 5267–5286.
[15] B.S. Thomas, R.C. Guptas, A comprehensive review on the applications of waste tire rubber in cement concrete, Renewable and Sustainable Energy Reviews Name 54 (2016) 1323–1333.
[16] S. Ramarad, M. Khalid, C. Ratnam, A.L. Chuah, W. Rashmis, Waste tire rubber in polymer blends: a review on the evolution, properties and future, Progress in Materials Science Name 72 (2015) 100–140.
[17] J. Wang, Q. Dai, R. Si, S. Guos, Mechanical, durability, and microstructural properties of macro synthetic polypropylene (PP) fiber-reinforced rubber concrete, Journal of Cleaner Production Name 234 (2019) 1351–1364.
[18] K. Liew, A. Akbars, The recent progress of recycled steel fiber reinforced concrete, Construction and Building Materials Name 232 (2020) 117232.
[19] M.A. Koroglu, Behavior of composite self-compacting concrete (SCC) reinforced with steel wires from waste tires, Rev. Constr. 17 (3) (2018) 484–498.
[20] A. Baricevic, D. Bjegovic, M. Skazlic, Hybrid fiber-reinforced concrete with unsorted recycled-tire steel fibers, J. Mater. Civ. Eng. 29 (6) (2017).
[21] M. Mastali, A. Dalvand, A.R. Sattarifard, Z. Abdollahnejad, M. Illikainen, Characterization and optimization of hardened properties of self consolidating concrete incorporating recycled steel, industrial steel, polypropylene and hybrid fibers, Compos. Part B-Eng. 151 (2018) 186–200.
[22] T. Almusallam, S.M. Ibrahim, Y. Al-Salloum, A. Abadel, H. Abbas, Analytical and experimental investigations on the fracture behavior of hybrid fiber reinforced concrete, Cem. Concr. Compos. 74 (2016) 201–217.
[23] D. Haripriya, G. Ganesh Naidu, Study of strength related resources of hybrid fiber reinforced concrete (HFRC) and energy absorption capacity (EAC), Mater. Today: Proc. 72 (2023) 2933–2938.
[24] Z. Al-Kamyani, F.P. Figueiredo, H. Hu, M. Guadagnini, K. Pilakoutas, Shrinkage and flexural behaviour of free and restrained hybrid steel fibre reinforced concrete, Constr. Build. Mater. 189 (2018) 1007–1018.
[25] A.A. Abdul Samad, N. Ali, N. Mohamad, J. Jayaprakash, K.F. Tee, P. Mendiss, Shear strengthening and shear repair of 2-span continuous RC beams with CFRP strips, Journal of Composites for Construction Name 21 (2017) 04016099.
[26] A.C. Aydins, Self compactability of high volume hybrid fiber reinforced concrete, Construction and Building Materials Name 21 (2007) 1149–1154.
[27] T. Asheghi Mehmandari, et al., Experimental and numerical analysis of tunnel primary support using recycled, and hybrid fiber reinforced shotcrete, Structures 63 (2024).
[28] O.P. Balogun, K.K. Alaneme, A.A. Adediran, I.O. Oladele, J.A. Omotoyinbo, K.F. Tee, Evaluation of the physical and mechanical properties of Short Entada mannii-glass fiber hybrid composites, Fibers Name 10 (2022) 30.
[29] A. Naseri, B. Maleki, T. Asheghi Mehmandari, A. Tohidi, A. Fahimifar, Investigating the influence of sample geometric variations on mechanical characterization in rock and concrete, J. Mining Environ. (2024).
[30] Ö. Ündül, F. Amann, N. Aysal, M.L. Plötzes, Micro-textural effects on crack initiation and crack propagation of andesitic rocks, Engineering Geology Name 193 (2015) 267–275.
[31] X. Shen, E. Brühwilers, Influence of local fiber distribution on tensile behavior of strain hardening UHPFRC using NDT and DIC, Cement and Concrete Research Name. 132 (2020) 106042.
[32] Ahmed M. Maglad, et al., Experimental and analytical investigation of fracture characteristics of steel fiber-reinforced recycled aggregate concrete, International Journal of Concrete Structures and Materials 17 (1) (2023) 74.
[33] J. Yates, M. Zanganeh, Y. Tais, Quantifying crack tip displacement fields with DIC, Engineering Fracture Mechanics Name 77 (2010) 2063–2076.
[34] D.A.S. Rambo, Y. Yao, F. de Andrade Silva, R.D. Toledo Filho, B. Mobashers, Experimental investigation and modelling of the temperature effects on the tensile behavior of textile reinforced refractory concretes, Cement and Concrete Composites Name 75 (2017) 51–61.
[35] M.A. Vicente, G. Ruiz, D.C. González, J. Mínguez, M. Tarifa, X. Zhangs, CT-Scan study of crack patterns of fiber-reinforced concrete loaded monotonically and under low-cycle fatigue, International Journal of Fatigue Name 114 (2018) 138–147.
[36] J. Minguez, D. González, M. Vicentes, Influence of fibre volume fraction and fibre orientation on the residual flexural tensile strength of fibre-reinforced concrete, Hormigón y Acero Name 70 (2019) 15–21.
[37] G.L. Balázs, O. Czoboly, É. Lublóy, K. Kapitány, Á. Barsis, Observation of steel fibres in concrete with Computed Tomography, Construction and Building Materials Name 140 (2017) 534–541.
[38] E. Pastorelli, H. Herrmann, Time-efficient automated analysis for fibre orientations in steel fibre reinforced concrete, Proceedings of the Estonian Academy of Sciences Name 65 (2016) 28.
[39] H. Herrmann, E. Pastorelli, A. Kallonen, J.-P. Suuronen, Methods for fibre orientation analysis of X-ray tomography images of steel fibre reinforced concrete (SFRC), Journal of materials science Name 51 (2016) 3772–3783.
[40] T. Ponikiewski, J. Katzers, X-ray computed tomography of fibre reinforced self-compacting concrete as a tool of assessing its flexural behaviour, Materials and Structures Name 49 (2016) 2131–2140.
[41] Ru Mu, et al., Effect of the orientation of steel fiber on the strength of ultra-high-performance concrete (UHPC), Construct. Build. Mater. 406 (2023) 133431.
[42] Xuhui Zhang, et al., Orientation of steel fibers in concrete attracted by magnetized rebar and its effects on bond behavior, Cement Concr. Compos. 138 (2023) 104977.
[43] J.D. Rios, H. Cifuentes, C. Leiva, S. Seitls, Analysis of the mechanical and fracture behavior of heated ultra-high-performance fiber-reinforced concrete by X-ray computed tomography, Cement and Concrete Research Name 119 (2019) 77–88.
[44] M. Miletić, L.M. Kumar, J.-Y. Arns, A. Agarwal, S.J. Foster, C. Arns, D. Perićs, Gradient-based fibre detection method on 3D micro-CT tomographic image for defining fibre orientation bias in ultra-high-performance concrete, Cement and Concrete Research Name. 129 (2020) 105962.
[45] T. Asheghi Mehmandari, A. Fahimifar, F. Asemi, The effect of the crack initiation and propagation on the P-wave velocity of limestone and plaster subjected to compressive loading, AUT Journal of Civil Engineering Name 4 (2020) 55–62.

[46] G.L. Golewskis, Estimation of the optimum content of fly ash in concrete composite based on the analysis of fracture toughness tests using various measuring systems, Construction and Building Materials Name 213 (2019) 142–155.
[47] G.L. Golewskis, Energy savings associated with the use of fly ash and nanoadditives in the cement composition, Energies Name 13 (2020) 2184.
[48] M. Mohammadifar, T. Asheghi Mehmandari, A. Fahimifars, Parametric and Sensitivity Analysis on the Effects of Geotechnical Parameters on Tunnel Lining in Soil Surrounding, مهندسی سازه و ساخت Name, 2024.
[49] S.C. Chin, K.F. Tee, F.S. Tong, S.I. Doh, J. Gimbuns, External strengthening of reinforced concrete beam with opening by bamboo fiber reinforced composites, Materials and Structures Name 53 (2020) 1–12.
[50] S. Diamond, J. Huangs, The ITZ in concrete–a different view based on image analysis and SEM observations, Cement and concrete composites Name 23 (2001) 179–188.
[51] P. Zare, T. Asheghi, A. Fahimifar, S. Zabetian, Experimental assessment of damage and crack propagation mechanism in heterogeneous rocks, Name 1 (2001) 1–16.
[52] T. Asheghi Mehmandari, D. Mohammadi, M. Ahmadi, M. Mohammadifar, Fracture mechanism and ductility performances of fiber reinforced shotcrete under flexural loading Insights from Digital image correlation (DIC), Insight-Civil Engineering 7 (1) (2024).
[53] E. Adili, A. Kheyroddins, Fiber interfacial transition zone concept for steel fiber-reinforced concrete by SEM observation, Journal of applied research and technology Name 19 (2021) 294–307.
[54] J. Němeček, Mikromechanické vlastnosti cementových kompozitů. České Vysoké Učení Technické V Praze, 2017.
[55] J. Němeček, V. Králík, V. Šmilauer, L. Polívka, A. Jager, Tensile strength of hydrated cement paste phases assessed by micro-bending tests and nanoindentation, Cement and Concrete Composites Name 73 (2016) 164–173.
[56] J. Němeček, V. Králík, J. Vondřejcs, Micromechanical analysis of heterogeneous structural materials, Cement and Concrete Composites Name 36 (2013) 85–92.
[57] A.I, Standard Specification for Portland Cement, in ASTM C150/C150M-21, ASTM ASTM, 2021.
[58] A.I., Standard test method for flexural performance of fiber-reinforced concrete (using beam with third-point loading), in: C1609/C1609M - 07, ASTM ASTM, 2022.
[59] Z.P. Bažant, J. Planas, Fracture and Size Effect in Concrete and Other Quasibrittle Materials, CRC Press, 1997.
[60] N. McCormick, J. Lords, Digital image correlation, Materials today Name 13 (2010) 52–54.
[61] N. Zhang, F. Wang, P. Li, Y. Liang, H. Luo, D. Ouyang, L. Luo, J. Wu, Y. Zhao, Y. Lis, Two-dimensional vertical-lateral hybrid heterostructure for ultrasensitive photodetection and image sensing, Materials Today Name 69 (2023) 79–87.
[62] T.M. Heenan, C. Tan, J. Hack, D.J. Brett, P.R. Shearings, Developments in X-ray tomography characterization for electrochemical devices, Materials Today Name 31 (2019) 69–85.
[63] J. Villanova, R. Daudin, P. Lhuissier, D. Jauffres, S. Lou, C.L. Martin, S. Labouré, R. Tucoulou, G. Martínez-Criado, L. Salvos, Fast in situ 3D nanoimaging: a new tool for dynamic characterization in materials science, Materials Today Name 20 (2017) 354–359.
[64] M. Celikins, The role of dynamic transmission electron microscopy on the development of next generation magnesium alloys, Materials Today Name 18 (2015) 472.
[65] E.A. Stachs, Real-time observations with electron microscopy, Materials Today Name 11 (2008) 50–58.